



HAL
open science

Additive manufacturing of polymer composites: Processing and modeling approaches

Ahmed El Moumen, Mostapha Tarfaoui, Khalid Lafdi

► To cite this version:

Ahmed El Moumen, Mostapha Tarfaoui, Khalid Lafdi. Additive manufacturing of polymer composites: Processing and modeling approaches. *Composites Part B: Engineering*, 2019, 171, pp.166-182. 10.1016/j.compositesb.2019.04.029 . hal-02125155

HAL Id: hal-02125155

<https://ensta-bretagne.hal.science/hal-02125155>

Submitted on 22 Oct 2021

HAL is a multi-disciplinary open access archive for the deposit and dissemination of scientific research documents, whether they are published or not. The documents may come from teaching and research institutions in France or abroad, or from public or private research centers.

L'archive ouverte pluridisciplinaire **HAL**, est destinée au dépôt et à la diffusion de documents scientifiques de niveau recherche, publiés ou non, émanant des établissements d'enseignement et de recherche français ou étrangers, des laboratoires publics ou privés.



Distributed under a Creative Commons Attribution - NonCommercial 4.0 International License

Additive manufacturing of polymer composites: processing and modeling approaches

A. El Moumen (a,*), M. Tarfaoui (a) and K. Lafdi (b)

(a) ENSTA Bretagne, IRDL - UMR CNRS 6027 Brest, France

(b) University of Dayton, Dayton, OH 45469-0168, United States.

*Corresponding author. E-mail address: ahmed.el_moumen@ensta-bretagne.fr,
mostapha.tarfaoui@ensta-bretagne.fr

Abstract:

Additive manufacturing, which is referred to as 3D printing, is a new developed process of fabricating metallic, ceramic, plastic and concrete materials. The goal of this article is to provide an overview of 3D printing processing methods and discuss their pros and cons. A comparison with other technologies such as injection molding and cutting-based machinery was discussed. Various modeling approaches and tools at all scale levels were depicted. We have presented a case study concerning the effect of pores formation in the mechanical properties of 3D printed polymer composites using FDM process. The mechanical behavior of 3D printed composites was determined using the homogenization technique based on the RVE notion. Recent uses of this technology in the area of electronics, aerospace and biomedical engineering were highlighted. Finally, important benefits and limitations were identified in order to clarify and motivate future works in this field.

Keywords: 3D printing, Additive Manufacturing of composites, Mechanical properties, Polymer-matrix composites.

1. Introduction

3D printing also referred as rapid prototyping or additive manufacturing, is a process of depositing matter layer by layer in order to fabricate net shape 3D objects [1, 2]. It is a two-step process: (1) creating 3D computer model using various graphics software and (2) printing using all kinds of technologies such as fused laminated object manufacturing, deposition modeling, selective laser sintering and stereolithography. These techniques provide all kind of benefits [3-4] including: (i) 3D printing enables product designs that are hard to create using the traditional manufacturing process. For example, GE Aviation Company used 3D printing technology to manufacture blade edges with complex designs in order to optimize airflow. Using ordinary manufacturing processes, it is difficult to fabricate such blade parts without increasing the cost and time. (ii) Reducing the energy consumption and the material usage. Modern industry, such as aerospace and military fields, built various parts using expensive materials such as titanium and diamond, and it takes an effort to reduce or recycle scrap produced during the machining of different parts. Using traditional manufacturing process, 80-90% of the original billet was lost [5]. (iii) 3D printing technology has the ability to fabricate multiple parts as a single element. Generally, it is easier to change and substitute, in term of cost and materials, a single product than a system composed of multiple parts. For example, GE Company manufactured a single part fuel nozzles using 3D printing technology; that requires the assembly of 20 components using the traditional manufacturing process [6].

The aerospace and military industries have adopted 3D printing of materials as a rapid and economical solution for manufacturing industrial components. As reported by Coykendall et al. [7], NASA used 70 3D printed parts for Mars Rover vehicles. These parts include flame retardant vents, camera mounts and housings. Also, NASA has already tested the possibility of 3D printing on the International Space Station, which allows astronauts to print tools in the station space when needed [8]. Boeing Company had printed 22000 components that are used in a variety of aircraft. European Aeronautic Defense and Space used 3D printing technology to build an optimized design of bracket, which will be used in Airbus A320. Many other sectors such as biomedical industry [9], automobile [10], construction and architectural fields [11] and food processing [12] are using 3D printing technology. The important aspects that distinguish 3D printing from other prototyping technologies are in cost reduction [13] and it is computer-based technology.

Before describing 3D printing technology, below some dates to show how the 3D printing was evolved.

- In 1986: Carl Deckard, Joe Beaman and Paul Forderhase developed the ideas of Chuck Hull and deposed a patent in the US on Selective Laser Sintering. The idea of Chuck Hull concerns the invention of a stereolithographic apparatus.
- In 1988: the fused deposition process was patented.
- In 1993: the Electron beam melting was patented.
- In 2005: the Paper 3D laminated printing was manufactured by Mcor Technologies Ltd and an Irish company.
- In 2008: MakerBot Industries was founded by Bre Pettis, Adam Mayer and Zach Hoeken. This company produces 3D printers.

In recent years, there has been considerable attention in developing 3D printing of polymer-based composite. In this paper, a brief introduction of 3D printing technique used for polymer composites was described. The improvements in properties were also discussed, in particular for last five years to show the progress in this area. Finally, we discuss the limitations of current technologies and some perspective.

2. Description of 3D printing technologies

3D printing consists of three basic steps:

- Step 1: a 3D solid model was computerized and converted into a standard file format (in general STL format).
- Step 2: the file is sent to a machine.
- Step 3: the part is manufactured layer by layer.

Figure 1 illustrates the overall 3D printing process of materials.

Various 3D printing techniques have been used to fabricate polymer based composites. Each technique has its own advantages and limitations. The selection of such technique depends mainly on material types, processing speed and performance.



Figure 1: 3D printing process flow (Graphic: Deloitte University Press).

2.1. Fused deposition modeling (FDM)

This technique is the most used for the fabrication of polymer-based materials. This technique was described in Crump's patent [14]. Polymer thermoplastic is extruded from a movable FDM head and then deposited layer by layer and then solidify into final parts. PC, PLA and ABS polymers are commonly used materials for this process. Figure 2 illustrates the schematic of the FDM process. The polymer is heated to 1°C above its melting point and solidifies immediately. The quality of printed parts is controlled by altering various printing parameters such as the thickness of the deposed layer, printing orientation, raster angle and air gap. Sood et al. [15] and Chacon et al. [16] studied the effect of processing parameters on the physical behaviors of composites. The quality of manufactured parts depends on many process variables (velocity, pressure, thickness of layers, temperature, printing angle and nature of polymers). The influence on mechanical responses such as tensile, impact response and flexural behaviors of printed specimens was studied [15]. Moreover, an increase in the number of deposited layers leads to an increase of the number of heating and cooling cycles. Consequently, residual stresses might occur which favors the interlayer cracking and delamination. In addition, small raster angles are not preferable for 3D printing of polymers according to results presented in [15].

FDM equipment requires a very low maintenance. However, it has some limitations such as poor surface quality [17], used mostly for thermoplastic polymers [18], slow process and delamination caused by temperature fluctuation [19]. Figure 3 demonstrates the capability of FDM technology in 3D printing large systems based fiber reinforcements and polymer resins.

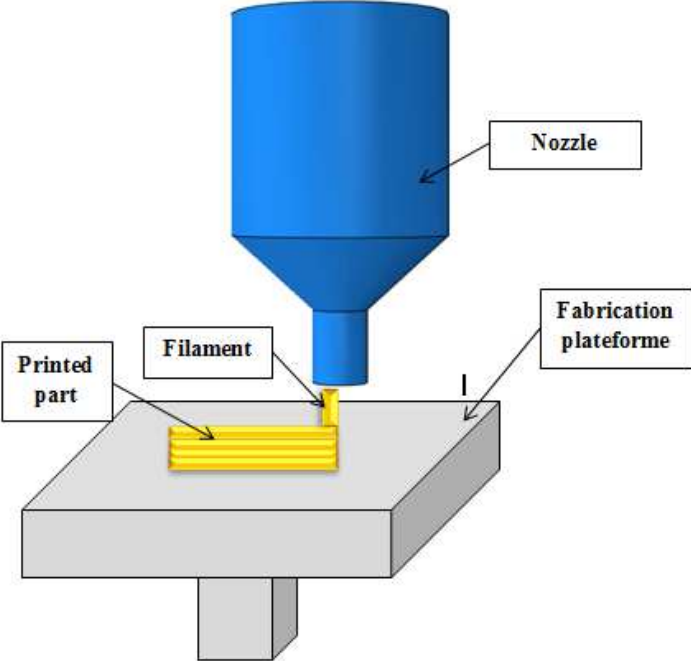


Figure 2: Schematic diagrams of fused deposition modeling (FDM).

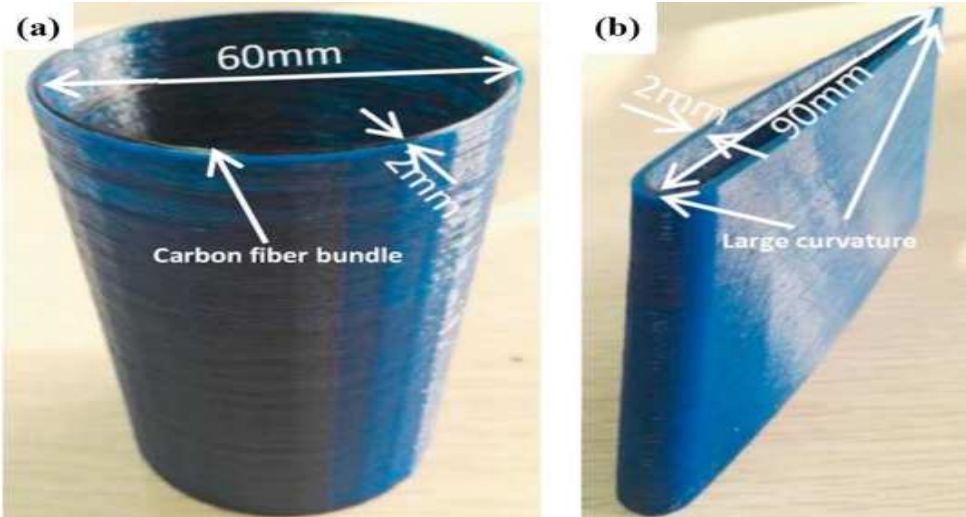


Figure 3: 3D imprinted system with FDM technology based on carbon fibers and PLA matrix [20].

2.2. Inkjet 3D printing (IJP)

The first patent for IJP was awarded on 1951 [21]. IJP technology was then modified and developed at Massachusetts Institute of Technology in 1993 as a rapid prototyping process [22]. This technology is based on powder processing and a jet was used to deposit matter onto paper. A quantity of ink in a chamber is ejected, via piezoelectric action, from a nozzle through a sudden reduction of the chamber volume. The droplet falls under the action of gravity and then dries through solvent evaporation. IJP is used for printing complex composites [23], scaffolds for tissue engineering [24-25] and ceramic component [26]. Some disadvantages of this technology include fragile print heads and expensive ink cartridges. Figure 4 illustrates the schematic presentation of the IJP process and an example of 3D printed part with IJP technology is presented in Figure 5.

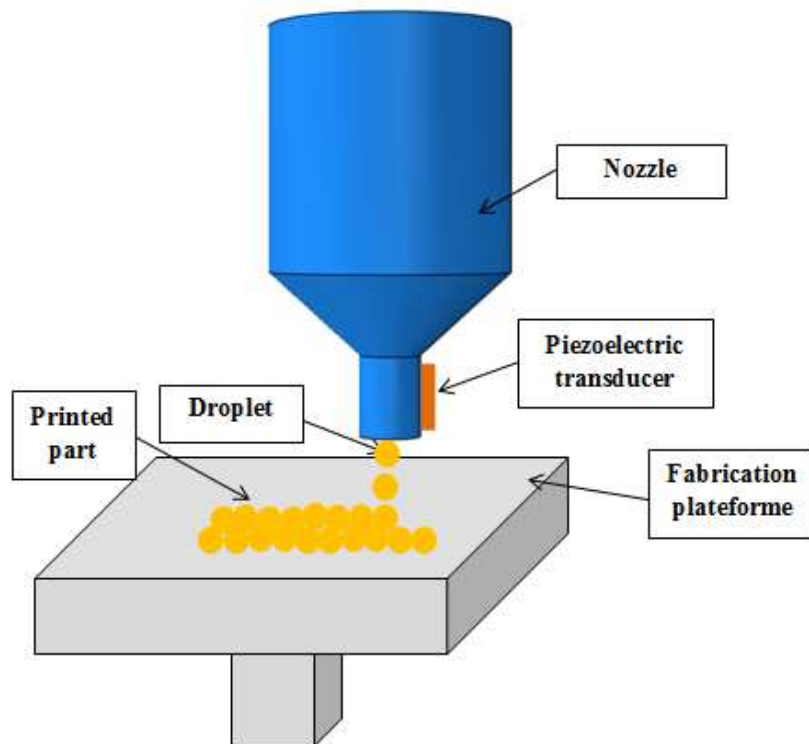


Figure 4: Schematic diagrams of IJP technology.

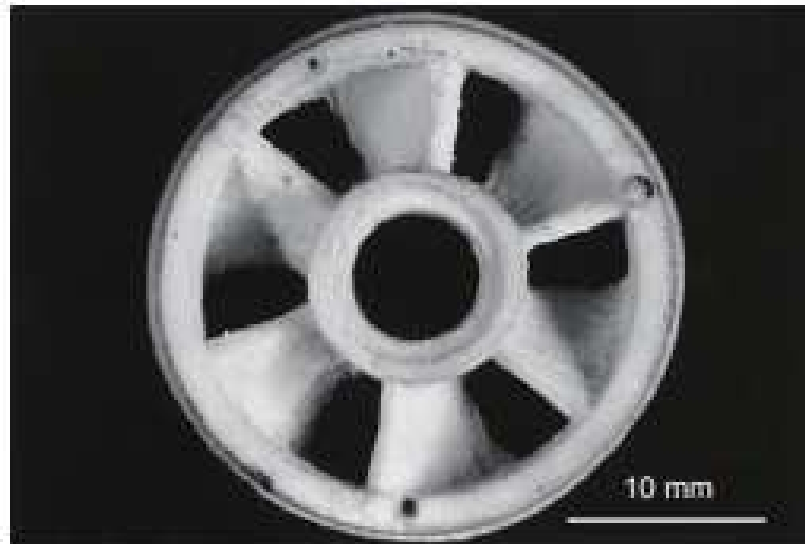


Figure 5: 3D printed part with IJP technology [27].

2.3. Stereolithography (SLA)

The patent for SLA was awarded in 1986 [28]. SLA technology uses UV light or an electron beam in order to initiate a chain reaction of the polymeric resin. Parts are produced by selectively UV curing a resin layer-by-layer. Acrylic and epoxy polymers are typically used materials in SLA. A post-treatment such as heating was used for printed parts with SLA to achieve a desired physical performance [25]. Figure 6 illustrates the schematic representation of SLA technology. The printed parts size is relatively small and no larger than a 2 cubic feet [3]. Also, the 3D components printed by SLA exhibit some mechanical property issues [29-33]. The photopolymer cost is prohibitive [30]. However, SLA prints high-quality parts [31-33]. An example of printed materials with SLA technique is shown in Figure 7.

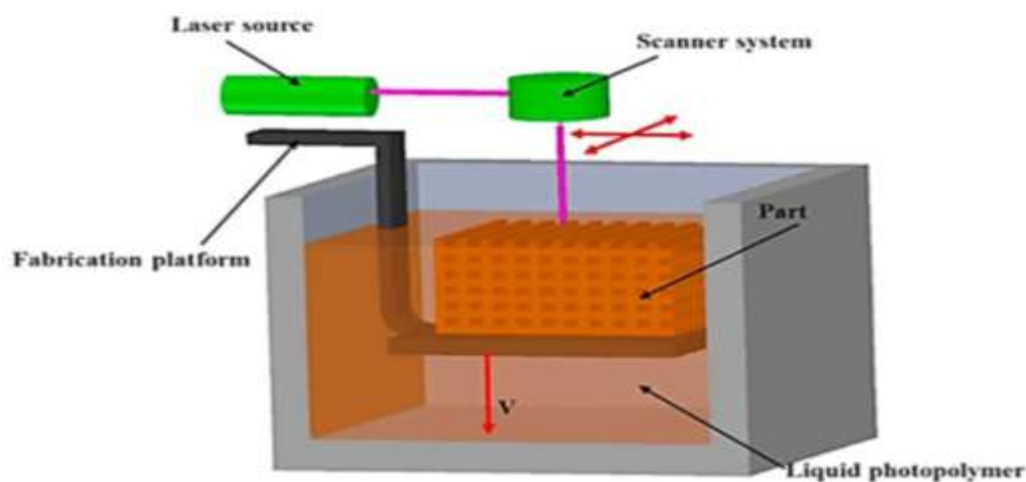


Figure 6: Schematic diagrams of SLA technology [33].



Figure 7: 3D printed system with SLA technology [34].

2.4. Selective laser sintering (SLS)

The process of SLS technology was described in Deckard and Beaman patents on September 1989 [35, 36]. In this technology, a high power laser source was used in order to fuse small particles of polymers. This technique is similar to IJP technologies. The powder is heated, slightly below its melting point in order to facilitate the fusion of different layers and to prevent thermal distortion. In the final product, unbounded powder should be removed to get the final part [37]. This technology relies on limited polymers [38] such as polyamide [39-41], polyethylene [42-43], PCL [44, 45] and PEEK [46]. Other limitations as the consolidation behavior and the molecular diffusion process of polymers need to be discussed. Figure 8 illustrates a schematic representation of the SLS technology. The laser scans the powder bed layer by layer to form 3D parts. Figure 9 shows an example of printed parts with SLS technology.

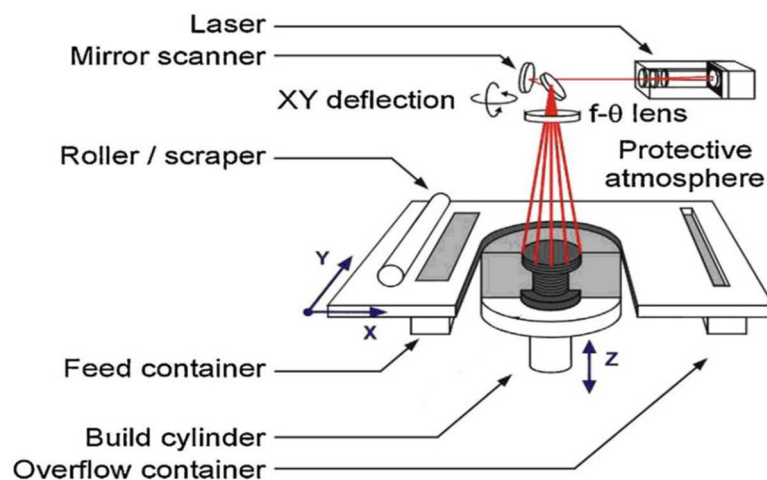


Figure 8: Schematic diagrams of SLS technology [47].



(a) Drill assembly printed in Nylon PA12 [48]



(b) Guitar created with selective laser sintering [49]

Figure 9: Example of printed polymers with SLS.

3. 3D printing of composites based polymers

Polymers and composites based polymers represent a major category of materials with potential for use in the 3D printing technology. These polymers include synthetic and biomaterial resins. The 3D printing technology involves polymers in various forms such as liquid and thermoplastic melts [50, 51].

Due to their physical properties, particle reinforcements are widely used in order to improve the properties of polymers such as ABS (butadiene styrene) [52-53], PLA (polylactic acid) [54-55], PC (polycarbonate) [56] as well as thermosetting resins like epoxy polymers. PLA and ABS are the main polymers tested in 3D printing of composites [57]. Most of the efforts were focused on the development of composites with short fiber reinforcements [58]. Glass fiber reinforced polypropylene (PP) was evaluated by Carneiro et al. [59] and the authors showed an improvement of 30% and 40% for the modulus and strength, respectively, compared to pure PP. Carbon nanotubes (CNTs) were used as an additive in ABS polymer and printed with FDM process [60]. The tensile strength of 5 wt% of CNTs filled FDM parts increased by 31%, but a dramatically decreased in the strain to failure. 3D printing of composites based particles was used to improve the tensile modulus by adding glass, iron and copper particles [61-63]. Improvement of dielectric permittivity and the wear resistance were reported using ceramic [64], tungsten [65] and aluminum oxide particles [66] to polymer resins. Türk et al. [67] characterized the thermo-mechanical performance of ABS reinforced with fibers. The printed parts were subjected to tensile and three-point bending tests to assess tensile Young's modulus, tensile yield strength and flexural modulus for the temperature up to

110 °C. Hao et al. [68] have characterized composite materials based on continuous carbon fibers reinforced thermosetting polymers using FDM 3D printing technology. Cong et al. [69] evaluated the effect of the length and weight ratio of carbon fiber on mechanical properties of printed parts with ABS resin using FDM process. An improvement in the tensile strength and Young's modulus was obtained with only 5 and 7.5 wt%. The results show that the longer carbon fibers provide the higher value in terms of strength and stiffness. Tian et al. [70] printed composite parts made of carbon fiber reinforced polylactide polymer. The fiber content was controlled by changing the process parameters during the printing of parts. When the concentration of fibers reached 27%, the modulus of 30 GPa and the flexural strength of 335 MPa were obtained. Similarly, Li et al. [71] investigated the mechanical properties of continuous carbon fiber reinforced polylactic acid composites fabricated using 3D printing technology. In this investigation, the authors have measured the mechanical strength and thermos-dynamic physical properties using DMA machine an electronic testing machine. The mechanical properties of printed composites were improved by adding the fibers into polymers. The same improvement trend was observed in [72-74]. An investigation by Tekinalp et al. [73] highlighted the challenges associated with using 3D printing of composites reinforced with fibers. The mechanical characterization of printed parts made from carbon fiber and ABS resin was discussed. The part was fabricated through FDM technology providing an increase in the strength and stiffness of specimens. Bakarich et al. [74] demonstrated the advantage to use of 3D printing in preparing composites based fibers and polymers. The utilization of this technology leads to enhancement of resins through modifying their mechanical properties such as Young's and shear moduli. Domingo-Espin et al. [75] studied the mechanical properties of 3D printed composites using numerical simulation tools. They were able to show a good correlation between numerical and experimental data.

Several authors have studied the effect of temperature on mechanical properties of 3D printed composites [76-79]. Kim et al. [76] studied the effect of the temperature of ABS polymers and observed 31.2% decrease in the tensile strength with temperatures up to 60 °C. Bagsik et al. [77] have characterized composites based Polyethylenimine for the case of elevated temperatures. Particles reinforced polymer composites fabricated by FDM using iron/ABS and copper/ABS, seems significantly improve the thermo-mechanical properties of 3D printed composites [78]. For printed composites with 30 vol% of copper particles, a storage modulus of 3.2 GPa was obtained at 90°C [79]. Recently, a composite structure

consists of microdiamond particles reinforced acrylate resins was made and tested. The mechanical and thermal properties of polymer were improved by adding 30% of microdiamond particles [80]. The temperature of the composite was higher compared to that of the pure polymer, thus demonstrating the improved heat transfer rates by the addition of nano-particles, Figure 10.

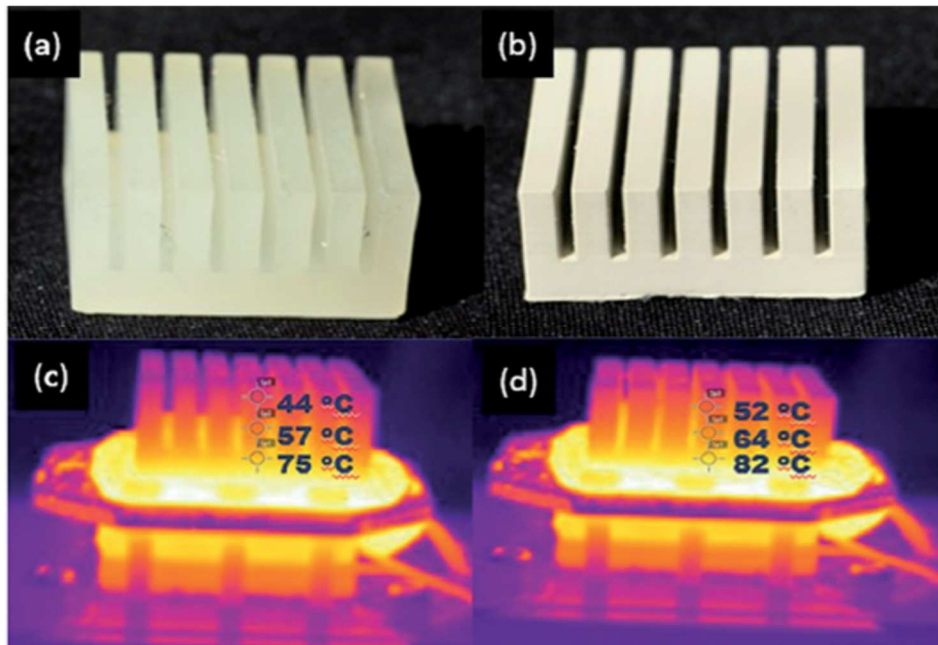


Figure 10: 3D printed composites: (a) only resin, (b) composite with 30% of micro-diamond particles and IR images of (c) polymer and (d) composite heated for 10 min at 100°C [80].

One challenge in 3D printing process remains is the distortion of parts, which is caused by the thermal expansion of polymers. An efficient solution is the adding metal particles into polymers [81]. When the ABS polymer is combined with iron and copper particles, the printed parts showed a large reduction in the thermal expansion coefficient, thus the distortion of the printed part reduced a lot. Other emerging composites for 3D printing are nanocomposites, which are capable of reducing thermal expansion coefficient and improving mechanical properties [82-86]. Postiglione et al. [87] developed a conductive nanocomposite film based on PLA and CNTs as presented in Figure 11. Weng et al. [88] characterized a 3D printing of nanocomposite reinforced with Nano SiO₂, attapulgite and montmorillonite particles. They concluded that SiO₂ exhibited the best physical properties. Boparai et al. [89] have studied the possibility of using a Nylon 6 based nanocomposite for 3D printing technology instead of ABS polymer. Using SEM, it was observed that the particles are uniformly dispersed and the Nylon 6 can be used as an alternative to ABS matrix. The

aggregation of particles during the printing process is still the main challenge [90]. Elliott et al. [91] investigated the effect of Quantum Dot nanoparticles onto photopolymer resin. QD is a type of nanoparticles which is 2–20 nm in diameter and is capable of absorbing ultraviolet light.

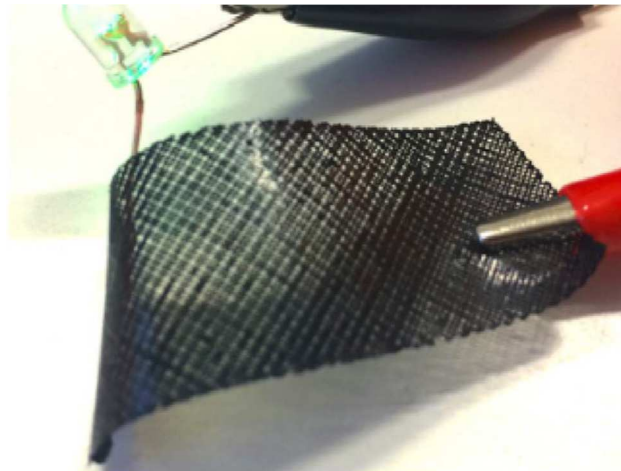


Figure 11: 3D printed nanocomposite based CNTs.

3D printing polymers might be used in the manufacturing of scaffolds for tissue engineering. These polymers include synthetic as poly (ethylene glycol) diacrylate or natural gelatin methacrylate [92]. An advantage of using synthetic polymers in 3D printing technology such as PLGA (poly(D, L-lactic-co-glycolic acid), and PCL (poly(ϵ -caprolactone) is that these materials have been approved by the FDA (Food and Drug Administration's) for clinical use [93]. 3D printing technology is relatively easy and provides a better-designed scaffold [94]. However, these conventional techniques suffer from several limitations including inadequate control over scaffold morphologies and properties such as pore geometry, pore size, agglomeration of pores and particles, and mechanical strength. Several tissues such as skin [95] and bladder [96] have been manufactured.

Inzana et al. [97] characterized 3D printed scaffolds, using ZPrinter® 450, for bone regeneration based on calcium phosphate and type I collagen and demonstrate the feasibility of this technology to enhance mechanical and cellular benefits in vitro. In other studies, a 3D printer was used to manufacture composite scaffolds consisting of PLA and bioactive CaP glass [98]. The printed composite scaffolds were shown in Figure 12. The incorporation of CaP glass improved cell adhesion of PLA by increasing both the hydrophilicity and the

roughness of the composite scaffolds. Traditional technologies are incapable to control porosity of scaffolds. Also, other micro-particles such as tri-calcium phosphate (TCP) have been used to fabricate composite scaffolds through different 3D printing technologies [99-101].

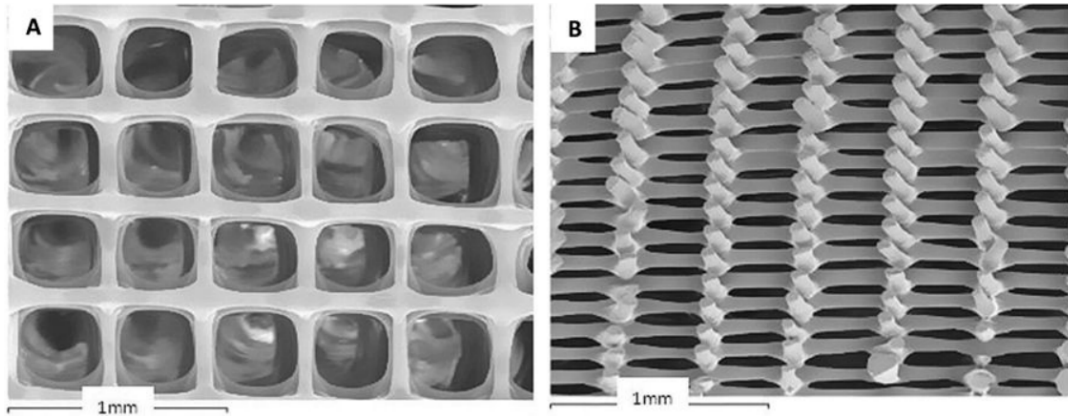


Figure 12: 3D printed composite scaffolds, images taken from [98].

To improve the strength of scaffolds, most of the manufactured composites were prepared by blending TCP with the polymer resin. Davila et al. [101] studied experimentally the composite scaffolds based on PCL reinforced with TCP. The results show that, in the case of the composite scaffold with 20 wt% of TCP, the compressive modulus increased 107% compared to that of the pure polymer scaffolds. Xia et al. [102] fabricated a composite reinforced with hydroxyapatite (HA) particles using SLS technique. In this study, 103% improvement was observed on the compressive strength of fabricated scaffolds. Other nanoparticles such as graphene [103], silica [104], CNTs [105] Fe_3O_4 [106] were also used to improve the strength and the compressive modulus of scaffolds. Recently, the mechanical behavior of a 3D printed PLA/HA composite scaffold was experimental investigated by Senatov et al. under fatigue tests [107]. During the test, the accumulation of plastic deformation and the formation of defects were observed in tested specimens. The incorporation of HA particles increased the crack resistance of scaffolds.

A comprehensive review of 3D printed composites for tissue engineering has been published in the open literature [108]. To date, the majority of researches on 3D printed scaffolds were focused mostly on bone tissues. Therefore more research is lacking in the field of tissue engineering with respect to other tissues such as cardiac tissue. The research in this field is necessary as different types of tissue replacements require different specifications such as specific mechanical properties, specific pore sizes and specific morphologies. 3D printing

of polymers reinforced with particles and fibers were used in different applications. Table 1 summarizes various particle reinforced polymer composites manufactured with 3D printing technology and the properties improvements of resulting composites [33] and Table 2 presents some applications of 3D printed composites.

Technique	3D printed composites	Enhancement in properties	Reference
FDM	TiO ₂ /ABS	Improved tensile modulus and strength	[109]
	Carbon nanofibers/ABS	Improved physical properties	[60]
	Montmorillonite/ABS	Improved tensile modulus and strength, flexural modulus and strength, thermal stability and reduced thermal expansion coefficient	[88]
	Graphene/ABS	Improved thermal and electrical conductivities	[110]
	Carbon nanofiber/ Graphite/ polystyrene	Improved electrical properties	[111]
SLA	CNT/epoxy	Improved tensile strength and reduced of the elongation	[112]
	Graphene oxide/photopolymer	Improved tensile modulus and strength	[113]
	TiO ₂ /epoxy acrylate	Improved tensile modulus and strength, flexural strength and hardness	[114]
	BaTiO ₃ /PEGDA	Improved piezoelectric coefficient	[115]
	CNT/acrylic ester	Improved the coefficient of electromagnetic energy absorption	[116]
	BST/epoxy	improved thermal conductivity	[117]
SLA	Carbon black/nylon-12	Improved electrical conductivity	[118]
	TiO ₂ /nylon-12 and graphite/ nylon-12	Improved tensile modulus and reduced the elongation	[119]
	Silica/Nylon-11	Improved tensile and compressive properties	[120]

Table 1: A summary of 3D printing techniques with improved physical properties.

Technique	3D printed composites	Applications	Reference study
FDM	HA/PLA	Biodegradable scaffold with improved crack resistance during cyclic loading	[107]
	HA/TCP	scaffold with improved compressive strength	[121]

Table 2: Manufactured composites with 3D printing technology and some applications.

As a new advanced manufacturing technology, 3D printing technology was studied by academics and practitioners. However, investigations are mostly interested in the process and their applications in different industries. In the next section, we have interested to modeling of the mechanical properties of 3D printed.

4. Numerical and analytical models for 3D printed composites

Four types of polymer composites can be produced by 3D technologies. These composites include: (1) Nano/Micro-particles reinforced polymers, (2) short fibers reinforced polymers, (3) unidirectional fibers reinforced polymers and (4) laminate polymer composites. These composites can be analyzed using existing analytical theories based on the micromechanical models or by using finite element theories. SEM microstructures of 3D printed composites differ from those prepared by traditional manufacturing techniques and there is a demand for modeling of these structures.

The intent of this section was not to provide an exhaustive review of all available analytical models in the open literature, but rather to suggest potential methods to estimate mechanical properties of 3D printed composites.

4.1. Particles reinforced polymer composites

4.1.1. Analytical bounds for particles reinforced polymers

There are several theories to predict the mechanical properties of rigid particles reinforced polymer composites. Mechanical properties of such composites can be calculated using the simple method based on the rule of mixtures [122-123] known as Voigt-Reuss (VR) bounds. Other popular existing approaches will be assessed in the isotropic composite namely: Hashin-Shtrikma bounds [124], the third order bounds (3OB) [125-126], Mori-Tanaka model [127], the Smallwood model [128] and Guth-Gold model [129]. Effective properties can be bounded with VR bounds using the simple equation:

$$E^v = pE_i + (1 - p)E_m \quad (1)$$

Where p is the volume fraction of the particles and E_i and E_m represents Young's moduli of the particles and matrix, respectively.

VR bounds are typically far apart, and do not provide exact solutions except in the cases of small volume fractions. Better universal bounds are given in other investigations.

Improved bounds for mechanical properties of particles reinforced polymers were developed in 1963 by Hashin and Shtrikman (HS) using the vibrational principles approaches. Based on these theories, they developed better mathematical laws than VR bounds for isotropic microstructures. For a two-phase composite, we have:

$$k^- = k_m + \frac{p}{\frac{1}{K_i - K_m} + \frac{3(1-p)}{(3K_m + 4G_m)}} \quad (2)$$

$$k^+ = k_i + \frac{1-p}{\frac{1}{K_m - K_i} + \frac{3p}{(3K_i + 4G_i)}} \quad (3)$$

$$G^- = G_m + \frac{p}{\frac{1}{G_i - G_m} + \frac{6(1-p)(K_m + 2G_m)}{5G_m(3K_m + 4G_m)}} \quad (4)$$

$$G^+ = G_i + \frac{1-p}{\frac{1}{G_m - G_i} + \frac{6p(K_i + 2G_i)}{5G_i(3K_i + 4G_i)}} \quad (5)$$

Where k_i , G_i and k_m , G_m are the bulk and shear moduli for the particles “i” and matrix “m”, respectively, while p represents the volume fraction of particles. The symbol “+ and -“ indicates the upper and lower bounds. Finally, having the value of bulk and shear moduli, the Young's modulus of the composite can be bounded using this equation:

$$E^\pm = \frac{9K^\pm}{3K^\pm + G^\pm} \quad (6)$$

The third order bounds (3OB) are the most sophisticated analytical bounds for the estimation of mechanical properties of particles reinforced polymers. These bounds depend on the properties of each phase, the volume fraction of the reinforcements, the shape and the distribution of the particles, and the morphological function ξ which describe the distribution

of particles. These bounds were proposed by Beran et al. [125] and Milton et al. [126] and summarized by Torquato et al. [130] for different types of composites.

In this section, we have used the Torquato notation and before presenting the 3OB, it is useful to introduce some notation for any arbitrary variable X :

$$\langle X \rangle = X_1\phi_1 + X_2\phi_2 \quad (7)$$

$$\langle \tilde{X} \rangle = X_1\phi_2 + X_2\phi_1 \quad (8)$$

$$\langle X \rangle_\xi = X_1\xi_1 + X_2\xi_2 \quad (9)$$

$$\langle X \rangle_\eta = X_1\eta_1 + X_2\eta_2$$

Where $\xi_1 = 1 - \xi_2$ and $\eta_1 = 1 - \eta_2$ are the morphological functions with mathematical expressions defined in [131]. The simplified forms of the 3OB on the effective bulk and shear moduli are given by equations:

$$k^- = \left[\langle \frac{1}{k} \rangle - \frac{\phi_1\phi_2(\frac{1}{k_2} - \frac{1}{k_1})^2}{\langle \frac{1}{\tilde{k}} \rangle + \langle \frac{1}{G} \rangle_\xi} \right]^{-1} \quad (10)$$

$$k^+ = \left[\langle k \rangle - \frac{\phi_1\phi_2(k_2 - k_1)^2}{\langle \tilde{k} \rangle + \langle G \rangle_\xi} \right] \quad (11)$$

and

$$G^- = \left[\langle \frac{1}{G} \rangle - \frac{\phi_1\phi_2(\frac{1}{G_2} - \frac{1}{G_1})^2}{\langle \frac{1}{\tilde{G}} \rangle + \Xi} \right]^{-1} \quad (12)$$

$$G^+ = \left[\langle G \rangle - \frac{\phi_1\phi_2(G_2 - G_1)^2}{\langle \tilde{G} \rangle + \Theta} \right] \quad (13)$$

$$\Theta = \frac{[2 \langle k \rangle_\xi \langle G \rangle^2 + \langle k \rangle^2 \langle G \rangle_\eta]}{\langle k + 2G \rangle} \quad (14)$$

$$\Xi = 2 \langle \frac{1}{k} \rangle_\xi + \langle \frac{1}{G} \rangle_\eta \quad (15)$$

In order to determine the Young's modulus bounds with 3OB, the equation (16) was used.

$$E^{\pm} = \frac{9K^{\pm}}{3K^{\pm} + G^{\pm}} \quad (16)$$

4.1.2. Direct analytical models for particles reinforced polymers

Mechanical properties of 3D printed polymer composites can be calculated using direct analytical estimates of Mori-Tanaka (MT) model. Using MT formulations, bulk and shear moduli as obtained as below:

$$k^{MT} = km \left(1 + \frac{p(Ki - Km)}{Km + a(1-p)(Ki - Km)} \right) \quad (17)$$

$$G^{MT} = Gm \left(1 + \frac{p(Gi - Gm)}{Gm + b(1-p)(Gi - Gm)} \right) \quad (18)$$

$$a = \frac{3Km}{3Km+4Gm} \quad \text{and} \quad b = \frac{6(Km+2Gm)}{5(3Km+4Gm)} \quad (19)$$

In 1979 Christensen and Lo [132] developed an elegant equation to determine the elastic moduli of two-phase composites. The formulation was proposed for bulk and shear moduli of composites and can be used for 3D printed polymer reinforced with rigid particles. For shear modulus, the estimated properties by generalized self-consistent (GSC) is the solution of the equation (20):

$$\mathbf{A} \left(\frac{G^{GSC}}{G_m} \right)^2 + \mathbf{B} \left(\frac{G^{GSC}}{G_m} \right) + \mathbf{C} = 0 \quad (20)$$

$$\begin{aligned} \mathbf{A} = & 8 \left(\frac{G_i}{G_m} - 1 \right) (4 - 5v_m) \eta_1 p^{\frac{10}{3}} - 2 \left(63 \left(\frac{G_i}{G_m} - 1 \right) \eta_2 + 2\eta_1 \eta_3 \right) p^{\frac{7}{3}} + \\ & 252 \left(\frac{G_i}{G_m} - 1 \right) \eta_2 p^{\frac{5}{3}} - 50 \left(\frac{G_i}{G_m} - 1 \right) (1 - 12v_m + 8v_m^2) \eta_2 p + 4(7 - \\ & 10v_m) \eta_2 \eta_3 \end{aligned} \quad (21)$$

$$\begin{aligned} \mathbf{B} = & -4 \left(\frac{G_i}{G_m} - 1 \right) (1 - 5v_m) \eta_1 p^{\frac{10}{3}} + 4 \left(63 \left(\frac{G_i}{G_m} - 1 \right) \eta_2 + 2\eta_1 \eta_3 \right) p^{\frac{7}{3}} - \\ & 504 \left(\frac{G_i}{G_m} - 1 \right) \eta_2 p^{\frac{5}{3}} + 150 \left(\frac{G_i}{G_m} - 1 \right) (3 - v_m) v_m \eta_2 p + 3(15v_m - \\ & 7) \eta_2 \eta_3 \end{aligned} \quad (22)$$

$$\begin{aligned} C = & 4 \left(\frac{G_i}{G_m} - 1 \right) (5v_m - 7) \eta_1 p^{\frac{10}{3}} - 2 \left(63 \left(\frac{G_i}{G_m} - 1 \right) \eta_2 + 2\eta_1 \eta_3 \right) p^{\frac{7}{3}} + \\ & 252 \left(\frac{G_i}{G_m} - 1 \right) \eta_2 p^{\frac{5}{3}} + 25 \left(\frac{G_i}{G_m} - 1 \right) (v_m^2 - 7) \eta_2 p - (7 + 5v_m) \eta_2 \eta_3 \end{aligned} \quad (23)$$

$$\eta_1 = \left(\frac{G_i}{G_m} - 1 \right) (49 - 50v_i v_m) + 35 \left(\frac{G_i}{G_m} \right) (v_i - 2v_m) + 35(2v_i - v_m) \quad (24)$$

$$\eta_2 = \left(\frac{G_i}{G_m} \right) (7 + 5v_i) + 4(7 - 10v_i) \quad (25)$$

$$\eta_3 = \left(\frac{G_i}{G_m} \right) (8 - 10v_m) + (7 - 5v_m) \quad (26)$$

For the bulk modulus, we have:

$$k^{GSC} = k_m + \frac{p(k_i - k_m)}{1 + (1 - p) \frac{(k_i - k_m)}{(k_m + \frac{4}{3}G_m)}} \quad (27)$$

4.2. Unidirectional fibers reinforced polymer composites

There are several analytical models for predicting the mechanical properties of 3D printed long unidirectional (UD) fibers reinforced polymer composites. These composites were considered as transversely isotropic materials, Figure 13. The stiffness tensor is defined in the elastic part by five independent constants. The mechanical properties were calculated from those of constituents.



Figure 13: Example of 3D printed UD fiber composites [133].

Different researches have been interested to the prediction of the mechanical properties of such composites. Halpin and Tsai [134] developed a famous theory for UD fiber composites, in which, the longitudinal moduli E_{11} , transverse moduli E_{22} and other properties are expressed as:

$$\left\{ \begin{array}{l} E_{11} = pE_i + (1 - p)E_m \\ E_{22} = E_m \left(\frac{1 + p\eta\zeta}{1 - p\eta} \right) \\ G_{12} = G_m \left(\frac{1 + p\eta\zeta}{1 - p\eta} \right) \end{array} \right. , \quad \eta = \frac{\frac{E_i}{E_m} - 1}{\frac{E_i}{E_m} - \zeta} \quad (28)$$

Where ζ is a shape parameter dependent on the geometry of the fiber and η is given by:

The Chamis model [135] proposed an analytical model which gives a formulation for all five elastic properties of UD composites. It is noticed that in this model, E_{11} is also predicted in the same manner of the Halpin-Tsai model.

$$\left\{ \begin{array}{l} E_{11} = pE_i + (1 - p)E_m \\ E_{22} = \frac{E_m}{1 - p \left(1 - \frac{E_m}{E_{22i}} \right)} \\ \nu_{12} = p\nu_{12i} + (1 - p)\nu_m \\ G_{12} = \frac{G_m}{1 - \sqrt{p} \left(1 - \frac{G_m}{G_{12i}} \right)} \\ G_{23} = \frac{G_m}{1 - \sqrt{p} \left(1 - \frac{G_m}{G_{23i}} \right)} \end{array} \right. \quad (29)$$

The Hashin and Rosen [136] model is another well-known theory that used to estimate the mechanical properties of UD fibers. The mechanical properties of these composites were expressed as:

$$\left\{ \begin{array}{l}
E_{11} = E_i p + E_m (1 - p) + \frac{4(v_i - v_m)^2}{\frac{1-p}{k_i} + \frac{p}{k_m} + \frac{1}{G_m}} p(1-p) \\
G_{12} = G_m \left(\frac{G_i(1+p) + G_m(1-p)}{G_i(1-p) + G_m(1+p)} \right) \\
G_{23} = G_i + \frac{1-p}{\frac{1}{G_m - G_i} + p \frac{k_i + 2G_i}{2G_i(k_i + G_i)}} \\
\vartheta_{12} = v_i p + v_m (1-p) + \frac{(v_i - v_m) \left(\frac{1}{k_m} - \frac{1}{k_i} \right)}{\frac{1-p}{k_i} + \frac{p}{k_m} + \frac{1}{G_m}} p(1-p) \\
k = k_m + \frac{p}{\frac{1}{k_i - k_m} + \frac{1}{\frac{1}{3}(G_i - G_m)} + \frac{(1-p)}{k_m + \frac{4}{3}G_m}} \\
\vartheta_{23} = \frac{k - mG_{23}}{k + mG_{23}}; \quad \text{with } m = 1 + 4k \frac{\vartheta_{12}^2}{E_{11}} \\
E_{22} = 2(1 + \vartheta_{23})G_{23}
\end{array} \right. \quad (30)$$

Where $k_i = \frac{E_i}{2(1-2\nu_i)(1+\nu_i)}$ and $k_m = \frac{E_m}{2(1-2\nu_m)(1+\nu_m)}$ are the bulk moduli of the fiber and the matrix, respectively.

4.3. Laminate composites

In order to predict the behavior of 3D printing composites, it is necessary to define the constitutive model that governs its mechanical behavior. Linear elasticity of laminate is described by the Hooke's law which gives the relationship between stress and strains. For an orthotropic 3D printed material, the compliance matrix has only nine terms and defined as:

$$\begin{pmatrix} \varepsilon_{11} \\ \varepsilon_{22} \\ \varepsilon_{33} \\ \gamma_{12} \\ \gamma_{23} \\ \gamma_{31} \end{pmatrix} = \begin{pmatrix} S_{11} & S_{12} & S_{13} & S_{14} & S_{15} & S_{16} \\ & S_{22} & S_{23} & S_{24} & S_{25} & S_{26} \\ & & S_{33} & S_{34} & S_{35} & S_{36} \\ & & & S_{44} & S_{45} & S_{46} \\ & & & & S_{55} & S_{56} \\ & & & & & S_{66} \end{pmatrix} = \begin{pmatrix} \sigma_{11} \\ \sigma_{22} \\ \sigma_{33} \\ \tau_{12} \\ \tau_{23} \\ \tau_{31} \end{pmatrix} \quad (31)$$

Where ε is the deformation, γ is the shearing strain, τ is the shearing stress and σ is the normal stress. Considering the conventional engineering constants, the equation (31) can be writing in terms of Young's modulus, Poisson ratio and shear modulus as:

$$\begin{pmatrix} \varepsilon_{11} \\ \varepsilon_{22} \\ \varepsilon_{33} \\ \gamma_{12} \\ \gamma_{23} \\ \gamma_{31} \end{pmatrix} = \begin{pmatrix} 1/E_{11} & -\nu_{12}/E_{11} & -\nu_{13}/E_{11} & 0 & 0 & 0 \\ & 1/E_{22} & -\nu_{23}/E_{22} & 0 & 0 & 0 \\ & & 1/E_{33} & 0 & 0 & 0 \\ & & & 1/G_{23} & 0 & 0 \\ & & & & 1/G_{13} & 0 \\ & & & & & 1/G_{12} \end{pmatrix} \begin{pmatrix} \sigma_{11} \\ \sigma_{22} \\ \sigma_{33} \\ \tau_{12} \\ \tau_{23} \\ \tau_{31} \end{pmatrix} \quad (32)$$

The compliance matrix is obtained by inverting the stiffness matrix, and we have:

$$\begin{pmatrix} \sigma_{11} \\ \sigma_{22} \\ \sigma_{33} \\ \tau_{12} \\ \tau_{23} \\ \tau_{31} \end{pmatrix} = \begin{pmatrix} C_{11} & C_{12} & C_{13} & C_{14} & C_{15} & C_{16} \\ & C_{22} & C_{23} & C_{24} & C_{25} & C_{26} \\ & & C_{33} & C_{34} & C_{35} & C_{36} \\ & & & C_{44} & C_{45} & C_{46} \\ & & & & C_{55} & C_{56} \\ & & & & & C_{66} \end{pmatrix} \begin{pmatrix} \varepsilon_{11} \\ \varepsilon_{22} \\ \varepsilon_{33} \\ \gamma_{12} \\ \gamma_{23} \\ \gamma_{31} \end{pmatrix} \quad (33)$$

Where

$$C_{11} = \frac{(S_{22} \cdot S_{33} - S_{23}^2)}{S}, C_{22} = \frac{(S_{11} \cdot S_{33} - S_{13}^2)}{S}, C_{33} = \frac{(S_{11} \cdot S_{22} - S_{12}^2)}{S} \quad (34)$$

$$C_{12} = \frac{(S_{23} \cdot S_{13} - S_{12} \cdot S_{33})}{S}, C_{13} = \frac{(S_{12} \cdot S_{23} - S_{22} \cdot S_{13})}{S}, C_{23} = \frac{(S_{12} \cdot S_{13} - S_{11} \cdot S_{23})}{S} \quad (35)$$

$$C_{44} = \frac{1}{S_{44}}, C_{55} = \frac{1}{S_{55}}, C_{66} = \frac{1}{S_{66}} \quad (36)$$

$$S = S_{11}S_{22}S_{33} + 2S_{12}S_{23}S_{13} - S_{13}^2S_{22} - S_{23}^2S_{11} - S_{12}^2S_{33} \quad (37)$$

4.3.1. Classical laminate theory

The classical laminate theory is an extension of the classical plate theory with some modifications to reflect the inhomogeneity in the thickness of composites. The classical laminate theory is applicable to all 3D printed composites that exhibit an orthogonal behavior. In this section, we present a summary of this theory. The stiffness tensor of each ply can be described as [137]:

$$Q_{ij} = \begin{bmatrix} Q_{11} & Q_{12} & 0 \\ Q_{12} & Q_{22} & 0 \\ 0 & 0 & Q_{66} \end{bmatrix} \quad (38)$$

Where

$$Q_{11} = \frac{E_{11}^2}{E_{11} - \vartheta_{12}^2 E_{22}}, Q_{22} = \frac{E_{11} E_{22}}{E_{11} - \vartheta_{12}^2 E_{22}}, Q_{12} = \frac{\vartheta_{12} E_{11} E_{22}}{E_{11} - \vartheta_{12}^2 E_{22}}, Q_{66} = G_{12} \quad (39)$$

The relation between stress and strain in the global axis and stress and strain in local axis can be obtained using transformation matrix as follow [137]:

$$\bar{Q}_{ij} = T^{-1} Q_{ij} T \quad (40)$$

Where

$$T = \begin{bmatrix} m^2 & n^2 & 2mn \\ n^2 & m^2 & -2mn \\ -mn & mn & m^2 - n^2 \end{bmatrix} \quad (41)$$

In which, $m = \cos\theta$, $n = \sin\theta$ and θ is the angle of the fiber. The elements of the transformed matrix are:

$$\begin{cases} \bar{Q}_{11} = Q_{11}m^4 + Q_{22}n^4 + 2(Q_{12} + 2Q_{66})m^2n^2 \\ \bar{Q}_{22} = Q_{11}n^4 + Q_{22}m^4 + 2(Q_{12} + 2Q_{66})m^2n^2 \\ \bar{Q}_{12} = (Q_{11} + Q_{22} - 4Q_{66})m^2n^2 + Q_{12}(m^2 + n^2) \\ \bar{Q}_{16} = (Q_{11} - Q_{22} - 2Q_{66})m^3n - (Q_{22} - Q_{12} - 2Q_{66})mn^3 \\ \bar{Q}_{26} = (Q_{11} - Q_{12} - 2Q_{66})m^3n - (Q_{22} - Q_{12} - 2Q_{66})nm^3 \\ \bar{Q}_{66} = (Q_{11} - Q_{22} - 2Q_{12} - 2Q_{66})m^2n^2 + Q_{66}(m^2 + n^2) \end{cases} \quad (42)$$

Then, coupling and bending stiffness tensors can be obtained by:

$$A_{ij} = \sum_{k=1}^n \bar{Q}_k (Z_k - Z_{k-1}) \quad (43)$$

$$B_{ij} = 1/2 \sum_{k=1}^n \overline{Q}_k (Z_k^2 - Z_{k-1}^2) \quad (44)$$

$$D_{ij} = 1/3 \sum_{k=1}^n \overline{Q}_k (Z_k^3 - Z_{k-1}^3) \quad (45)$$

Where z represents the vertical position in the composite ply.

The connection between the applied loads and the associated strains in the printed laminate was obtained as follows:

$$\begin{bmatrix} N \\ M \end{bmatrix} = \begin{bmatrix} A & B \\ B & D \end{bmatrix} \begin{bmatrix} \varepsilon^0 \\ k \end{bmatrix} \quad (46)$$

Where N is the normal stress resultant, ε^0 is the strain term in the midplane, M is the moment resultant and k is the twist of the laminate.

The $[A]$, $[B]$, and $[D]$ tensors are called the extensional, coupling, and bending stiffness tensors, respectively. Finally, the resultant force and the moment can be obtained in terms of the midplane strains and curvature as:

$$\begin{bmatrix} N_x \\ N_y \\ N_{xy} \end{bmatrix} = \begin{bmatrix} A_{11} & A_{12} & A_{16} \\ A_{12} & A_{22} & A_{26} \\ A_{13} & A_{26} & A_{66} \end{bmatrix} \begin{bmatrix} \varepsilon_x^0 \\ \varepsilon_y^0 \\ \gamma_{xy}^0 \end{bmatrix} + \begin{bmatrix} B_{11} & B_{12} & B_{16} \\ B_{12} & B_{22} & B_{26} \\ B_{13} & B_{26} & B_{66} \end{bmatrix} \begin{bmatrix} k_x \\ k_y \\ k_{xy} \end{bmatrix} \quad (47)$$

and

$$\begin{bmatrix} M_x \\ M_y \\ M_{xy} \end{bmatrix} = \begin{bmatrix} B_{11} & B_{12} & B_{16} \\ B_{12} & B_{22} & B_{26} \\ B_{13} & B_{26} & B_{66} \end{bmatrix} \begin{bmatrix} \varepsilon_x^0 \\ \varepsilon_y^0 \\ \gamma_{xy}^0 \end{bmatrix} + \begin{bmatrix} D_{11} & D_{12} & D_{16} \\ D_{12} & D_{22} & D_{26} \\ D_{13} & D_{26} & D_{66} \end{bmatrix} \begin{bmatrix} k_x \\ k_y \\ k_{xy} \end{bmatrix} \quad (48)$$

If the thermos-elastic strains are taken into account, the stress-strain relation of 3Dprinted composites can be written as follows:

$$\begin{bmatrix} \sigma_x \\ \sigma_y \\ \tau_{xy} \end{bmatrix} = \begin{bmatrix} \overline{Q}_{11} & \overline{Q}_{12} & \overline{Q}_{16} \\ \overline{Q}_{12} & \overline{Q}_{22} & \overline{Q}_{26} \\ \overline{Q}_{16} & \overline{Q}_{26} & \overline{Q}_{66} \end{bmatrix} \times \left(\begin{bmatrix} \varepsilon_x \\ \varepsilon_y \\ \gamma_{xy} \end{bmatrix} - \begin{bmatrix} \overline{\alpha}_x \Delta T \\ \overline{\alpha}_y \Delta T \\ \overline{\alpha}_{xy} \Delta T \end{bmatrix} \right) \quad (49)$$

Where

$$\begin{cases} \bar{\alpha}_x = \alpha_1 m^2 + \alpha_2 n^2 \\ \bar{\alpha}_y = \alpha_1 n^2 + \alpha_2 m^2 \\ \bar{\alpha}_{xy} = 2(\alpha_1 - \alpha_2)nm \end{cases} \quad (50)$$

By integrating the stress through the laminate thickness, the resultant force and moments are obtained as follows:

$$\begin{bmatrix} N \\ M \end{bmatrix} = \begin{bmatrix} A & B \\ B & D \end{bmatrix} \begin{bmatrix} \varepsilon^0 \\ k \end{bmatrix} - \begin{bmatrix} N^{\Delta T} \\ M^{\Delta T} \end{bmatrix} \quad (51)$$

According to [138] in order to avoid out of plane heat induced distortion, symmetric laminates have to be used. In fact, the B matrix vanishes. In the case of symmetric laminates under only thermal loading, N matrix also vanishes and therefore the strain expression can be obtained from the equation (51):

$$\varepsilon^0 = A^{-1} N^{\Delta T} \quad (52)$$

The laminate thermal expansion coefficient can be obtained:

$$\alpha = \frac{\varepsilon^0}{\Delta T} = \frac{A^{-1} N^{\Delta T}}{\Delta T} \quad (53)$$

Considering the thermal behavior in the x-direction, the expression of the thermal expansion coefficient was obtained from the equation (43) and (53):

$$\begin{aligned} \alpha_x = & A_{11}^{-1} \sum_{k=0}^n (\bar{Q}_{11} \bar{\alpha}_x + \bar{Q}_{12} \bar{\alpha}_y + \bar{Q}_{16} \bar{\alpha}_{xy}) (Z_k - Z_{k-1}) + \\ & A_{12}^{-1} \sum_{k=0}^n (\bar{Q}_{12} \bar{\alpha}_x + \bar{Q}_{22} \bar{\alpha}_y + \bar{Q}_{26} \bar{\alpha}_{xy}) (Z_k - Z_{k-1}) + A_{16}^{-1} \sum_{k=0}^n (\bar{Q}_{16} \bar{\alpha}_x + \\ & \bar{Q}_{26} \bar{\alpha}_y + \bar{Q}_{66} \bar{\alpha}_{xy}) (Z_k - Z_{k-1}) \end{aligned} \quad (54)$$

Where the tensor A is defined in the equation (43) and the expression of the $[A]^{-1}$ terms are [139]:

$$A_{11}^{-1} = \frac{A_{22}}{(A_{11}A_{22} - A_{12}^2)}, A_{12}^{-1} = \frac{-A_{12}}{(A_{11}A_{22} - A_{12}^2)}, A_{16}^{-1} = 0 \quad (55)$$

Additionally, the classical laminate theory can be used to evaluate the elastic constants of the 3D printed composites. In general case, the printed composite is associated with the void

formation which needs to be considered in the modeling of mechanical behaviors. Melenka et al. [140] developed an analytical model for 3D printed composites taken into account the voids formation. The expression of this model is:

$$\left\{ \begin{array}{l} E_{11} = (1 - \rho_1)E \\ E_{22} = (1 - \rho_1^{0.5})E \\ G_{12} = G \frac{(1 - \rho_1)(1 - \rho_1^{0.5})}{(1 - \rho_1) + (1 - \rho_1^{0.5})} \\ \nu_{12} = (1 - \rho_1)\nu \\ \nu_{21} = (1 - \rho_1^{0.5})\nu \end{array} \right. \quad (56)$$

Where E, G and ν are the elastic modulus, the shear moduli and Poisson ratio of the polymer.

4.3.2. MESOTEX model for 3D printed composites

MESOTEX model is an analytical model initially proposed by Scida et al. [141] with an objective of predicting 3D elastic properties of several ordinary laminate composites. Based on the classical laminate theory, the MESOTEX was used to analyze plain-weave, twill-weave and satin-weave (of 5 or 8) composites and their hybrid equivalents. It is proposed in this study for predicting the mechanical properties of 3D printed composites.

In this model, the periodicity of woven composites allows us to isolate a repeating unit-cell. In the unit-cell, each strand is described by a sinusoidal path for an undulating portion and the mechanical properties of composites are determined by discretizing each strand. The stiffness matrix [C] of each infinitesimal slice (strands and the resin element) is written as a summation of the stiffness of warp strand, fill strand and the resin [141]:

$$C_{ij}(x, y) = \sum_I V_I(x, y) \bar{Q}_{ij}^I(x, y), \quad (i, j = 1 \text{ to } 6) \quad (57)$$

Where \bar{Q}_{ij}^I is the transformed stiffness matrix, the 'I' refers to fill strand, warp strand and matrix and V_I is the 'I' element volume fraction in the slice. The 6x6 elements of the \bar{Q}_{ij}^I matrix are evaluated for the 'I' element as follows:

$$Q_{ij} = \begin{bmatrix} Q_{11}^I & Q_{12}^I & Q_{13}^I & 0 & 0 & 0 \\ Q_{21}^I & Q_{22}^I & Q_{23}^I & 0 & 0 & 0 \\ Q_{31}^I & Q_{32}^I & Q_{33}^I & 0 & 0 & 0 \\ 0 & 0 & 0 & Q_{44}^I & 0 & 0 \\ 0 & 0 & 0 & 0 & Q_{55}^I & 0 \\ 0 & 0 & 0 & 0 & 0 & Q_{66}^I \end{bmatrix} \quad (58)$$

In which

$$Q_{11}^I = \frac{1 - \vartheta_{23}^I \vartheta_{32}^I}{E_2^I E_3^I \Delta^I}, Q_{12}^I = Q_{21}^I = \frac{\vartheta_{21}^I + \vartheta_{23}^I \vartheta_{31}^I}{E_2^I E_3^I \Delta^I} = \frac{\vartheta_{12}^I + \vartheta_{32}^I \vartheta_{13}^I}{E_1^I E_3^I \Delta^I} \quad (59)$$

$$Q_{22}^I = \frac{1 - \vartheta_{13}^I \vartheta_{31}^I}{E_1^I E_3^I \Delta^I}, Q_{23}^I = Q_{32}^I = \frac{\vartheta_{32}^I + \vartheta_{12}^I \vartheta_{31}^I}{E_1^I E_3^I \Delta^I} = \frac{\vartheta_{23}^I + \vartheta_{21}^I \vartheta_{13}^I}{E_1^I E_2^I \Delta^I} \quad (60)$$

$$Q_{33}^I = \frac{1 - \vartheta_{12}^I \vartheta_{21}^I}{E_1^I E_2^I \Delta^I}, Q_{13}^I = Q_{31}^I = \frac{\vartheta_{31}^I + \vartheta_{21}^I \vartheta_{32}^I}{E_2^I E_3^I \Delta^I} = \frac{\vartheta_{13}^I + \vartheta_{12}^I \vartheta_{23}^I}{E_1^I E_2^I \Delta^I} \quad (61)$$

$$Q_{44}^I = G_{23}^I, \quad Q_{55}^I = G_{13}^I, \quad Q_{66}^I = G_{12}^I \quad (62)$$

$$\text{and } \Delta^I = \frac{1 - \vartheta_{12}^I \vartheta_{21}^I - \vartheta_{32}^I \vartheta_{23}^I - \vartheta_{13}^I \vartheta_{31}^I - 2\vartheta_{13}^I \vartheta_{21}^I \vartheta_{32}^I}{E_1^I E_2^I E_3^I} \quad (63)$$

In equation (63), the terms E_1^I, E_2^I, E_3^I are the three-dimensional elastic properties for the 'T' elements (matrix, fil or warp strand). The transformed stiffness matrix is calculated as:

$$[\bar{Q}_{ij}^I] = [T_{ij}^I]^{-1} [Q_{ij}^I] [R_{ij}] [T_{ij}^I] [R_{ij}]^{-1} \quad (64)$$

Where R and T are the Reuter matrix and the stress transformation matrix. These two matrices were given in [141].

Once the $[\bar{Q}_{ij}^I]$ terms are calculated, the $[C_{ij}]$ stiffness tensor can be evaluated for each slice using Equation (57). Consequently, the $[C_{ij}]_{global}$ matrix referred to the stiffness matrix averaged over the unit cell, including warp and fill strands and matrix regions, can be written as:

$$C_{ij} = \begin{pmatrix} C_{11} & C_{12} & C_{13} & 0 & 0 & 0 \\ & C_{22} & C_{23} & 0 & 0 & 0 \\ & & C_{33} & 0 & 0 & 0 \\ & & & C_{44} & 0 & 0 \\ & & & & C_{55} & 0 \\ & & & & & C_{66} \end{pmatrix} \quad (65)$$

Finally, the effective Young's modulus, shear moduli and Poisson's ratios of the 3D printed composite can be obtained as:

$$E_{11} = \frac{A}{h(A_{22}A_{33} - A_{23}^2)}, E_{22} = \frac{A}{h(A_{11}A_{33} - A_{13}^2)}, E_{33} = \frac{A}{h(A_{11}A_{22} - A_{12}^2)} \quad (66)$$

$$\nu_{xy} = -\frac{A_{13}A_{23} - A_{12}A_{33}}{A_{22}A_{33} - A_{23}^2}, \nu_{xz} = -\frac{A_{12}A_{23} - A_{13}A_{22}}{A_{22}A_{33} - A_{23}^2}, \nu_{yz} = -\frac{A_{12}A_{13} - A_{11}A_{23}}{A_{11}A_{33} - A_{12}^2} \quad (67)$$

$$G_{xy} = \frac{A_{66}}{h}, \quad G_{xz} = \frac{A_{55}}{h}, \quad G_{yz} = \frac{A_{44}}{h} \quad (68)$$

Where h is the composite thickness and

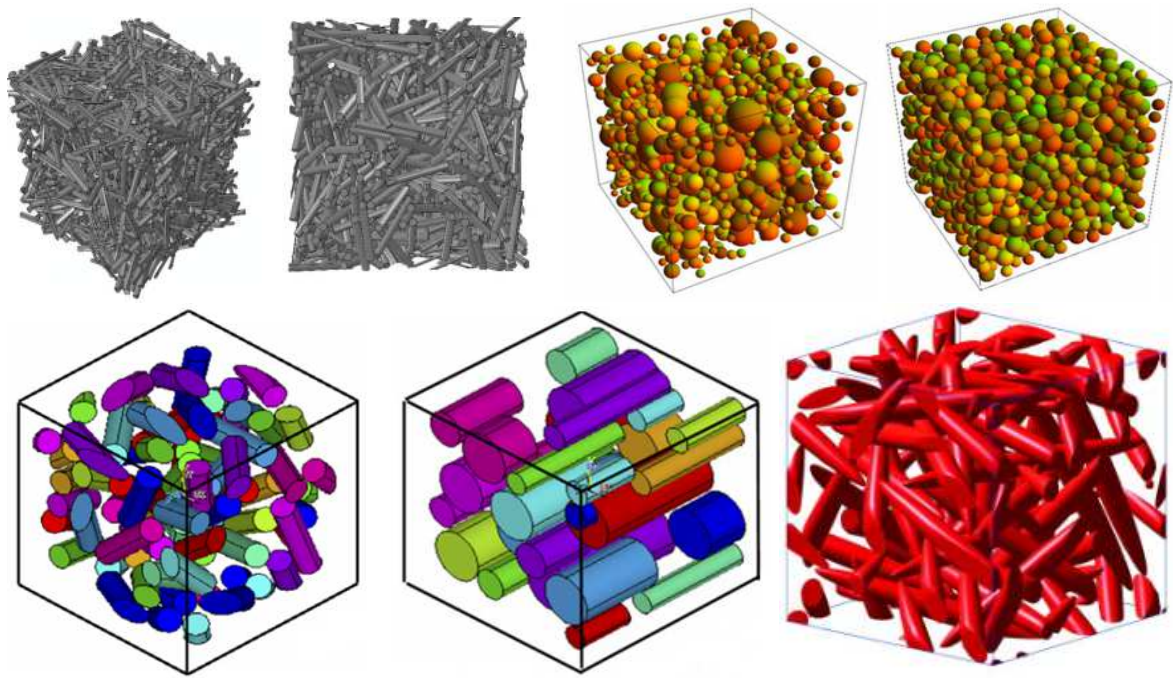
$$A = A_{11}A_{22}A_{33} + 2A_{12}A_{13}A_{23} - A_{13}^2A_{22} - A_{12}^2A_{33} - A_{23}^2A_{11} \quad (69)$$

5. Finite element modeling of 3D printed composites

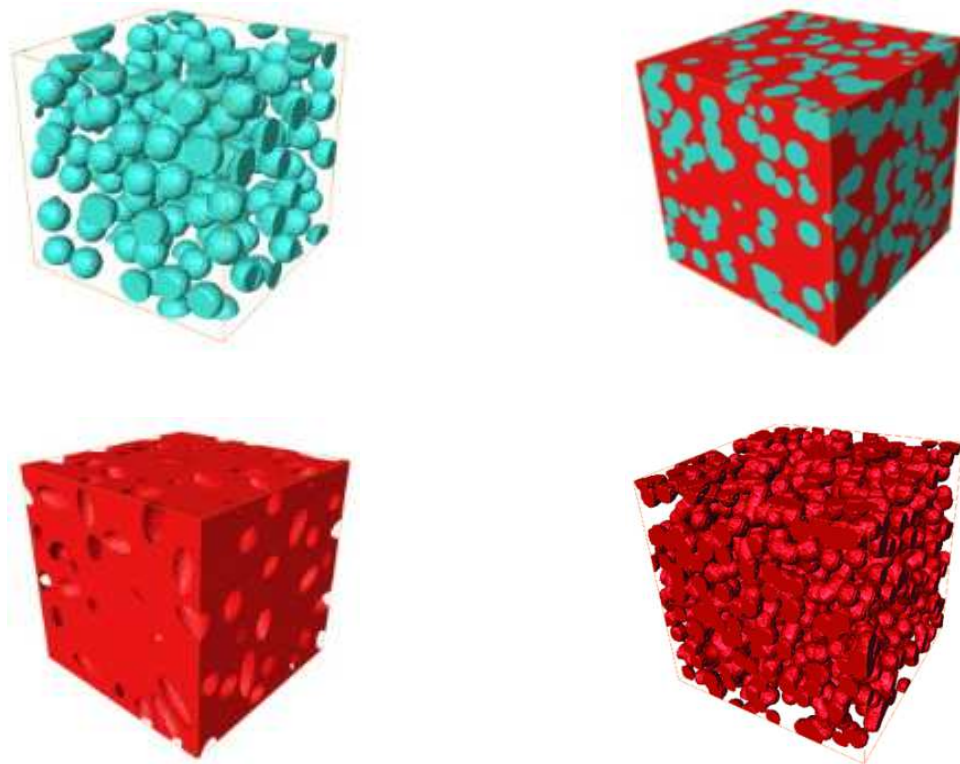
Finite element method (FEM) is particularly interesting for modeling 3D printed composites due to its capability to analyze different complex shape at micro and macroscales. This method was used for different types of composites namely, spherical and ellipsoidal particles reinforced polymer matrix [142, 143, 144, 145], natural aggregates reinforced the PLA polymer [146], short and long fibers reinforced composites [147, 148, 149], laminate composites [150, 151, 152], polymeric membrane [153] and nanoparticles reinforced composites [154, 155].

The primary distinction of 3D printed composites is the void formation during the manufacturing process and that needs to be incorporated into FE model based on the representative volume element (RVE) approach. This approach can be implemented and used for different 3D printing technology. The RVE is a cubic unit cell with single or multiple particles (inclusion, ellipses or fiber) embedded randomly or uniformly in the polymer matrix with a certain volume fraction similar to those of the printed composite. Generally, the unit cell (or RVE) depends upon the microstructures of materials. To generate this RVE, different algorithms were implemented in order to define a distribution of the particles in the space.

To model the RVE of a 3D printed polymer reinforced with particles, different investigations present various kinds of models adapted for these cases. Random Sequential Adsorption (RSA) algorithm and the Poisson process were the main used algorithm to create the RVE for modeling the behavior of composites reinforced with particles. Using these algorithms, the particles with certain shapes are randomly and sequentially distributed into polymer matrix space with or without overlap. First, random coordinates were generated for the center of one particle with a defined radius and deposited in the space. The next generated coordinates of particle centers were checked for non-overlapping condition with previously deposited particles. This process will be finished when the desired volume fraction is achieved. Figures 14, 15 and 16 give an example of generated microstructures, or RVE, for the numerical modeling of composites. This RVE can be used for the case of 3D printed composites. RVEs depend upon the microstructure parameter. Some common types are short fibers reinforced polymers, UD fibers reinforced particles and 3D braided microstructures. These techniques can be used for 3D printed polymer composites.



(a) RVE generated with RSA algorithm for different types of microstructures [156, 157, 158]



(b) RVE generated with Poisson process for different types of microstructures [142, 143, 159]

Figure 14: RVE models for particles reinforced 3D printed polymer composites.

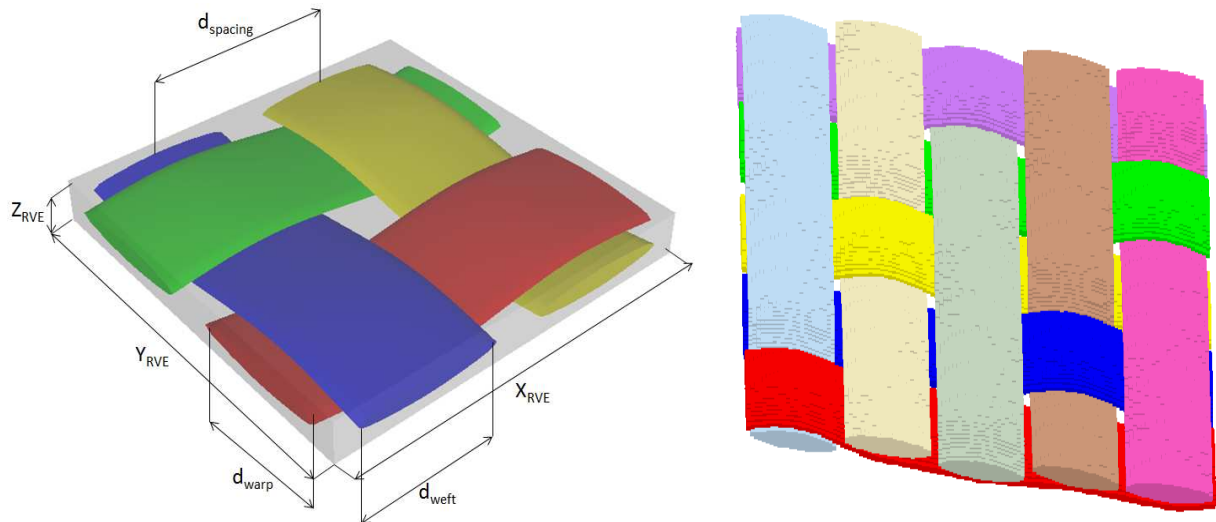


Figure 15: RVE models for laminated polymer composites [154].

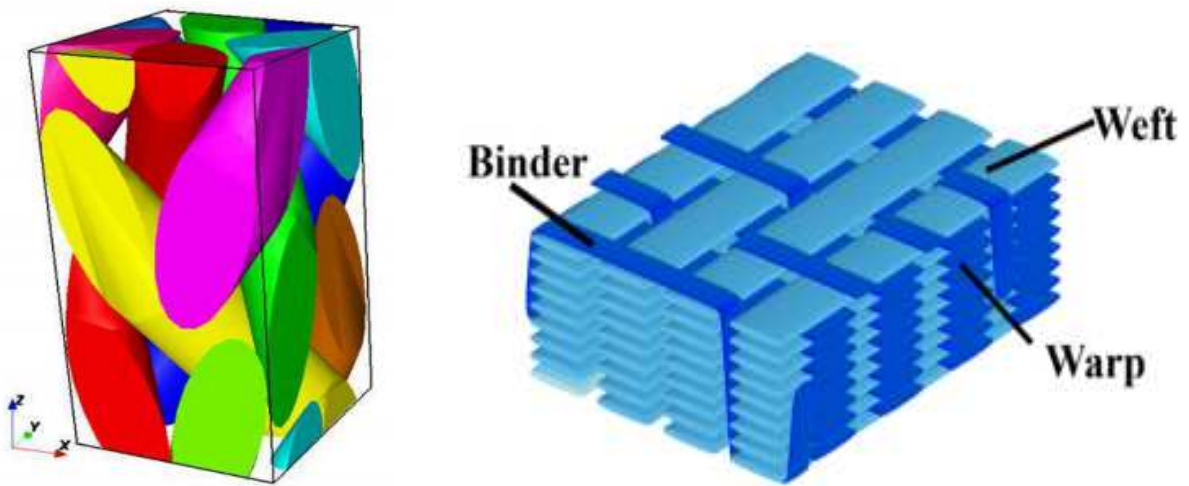


Figure 16: RVE models for 3D braided composites [160].

Another used approach for modeling of composites is multiscale RVE based on the real microstructure of SEM or μ -CT. This technique can be applied for 3D printed composites. Microscopic analysis using these techniques can increase the accuracy of the model, but is often too expensive. Figure 17 shows an example of the real RVE for numerical modeling of polymer composites.



(a) SEM microstructures [146]



(b) μ -CT microstructures [161]

Figure 17: RVE models based real microstructures for modeling polymer composites.

6. Case study and future works

One of the main drawbacks of 3D printing technology is the void formation of printed parts. The created porosity can thereby reduce the mechanical performance of printed composites. The concentration of these voids depends mainly on the process. For example, using FDM process, the formation of voids is more common and considered as the main factor that results in the reduction and anisotropic mechanical properties of composites which favors the delamination between layers of printed materials. Also, the anisotropic behavior was caused by the nature of layer by layer printing. The change in the texture and the morphology in the transverse direction of printed composites results in higher strength compared to the longitudinal direction. This phenomenon was observed for 3D printed polymers [162-163] and other materials [164]. For instance, the anisotropic of a 3D printed polymer composite can be achieved by controlling the formation and the distribution of the pores.

In this section, and for our future works, we are interested to study the effect of pores formation in the mechanical properties of 3D printed polymer composites. The mechanical behavior of the composites was determined using the homogenization technique based on the RVE notion. The RVE is constructed with the help of Poisson process or RSA algorithm. The pore volume fraction “p” in the 3D printed composite was determined from the SEM morphology using the pixel technique via the equation:

$$p = \frac{\sum_{i=1}^n S_i}{S_{lw}} \quad (70)$$

Where S_i is the area of pores and S_{lw} is the area of an SEM image and n is the number of pores in the SEM images. A schematic representation of the microstructure of 3D printed composite including the distribution of pores is depicted in Figure 18. Micrographs of 3D printed composites typically show a clear distribution of pores (random, rectangular or hexagonal distribution). In general cases, the random distribution of pores was considered. It is assumed that the particles are randomly distributed in the polymer. The number of the pores ‘ n ’ in the RVE can be obtained via the equation:

$$n = \frac{p V_{RVE}}{V_{pore}} \quad (71)$$

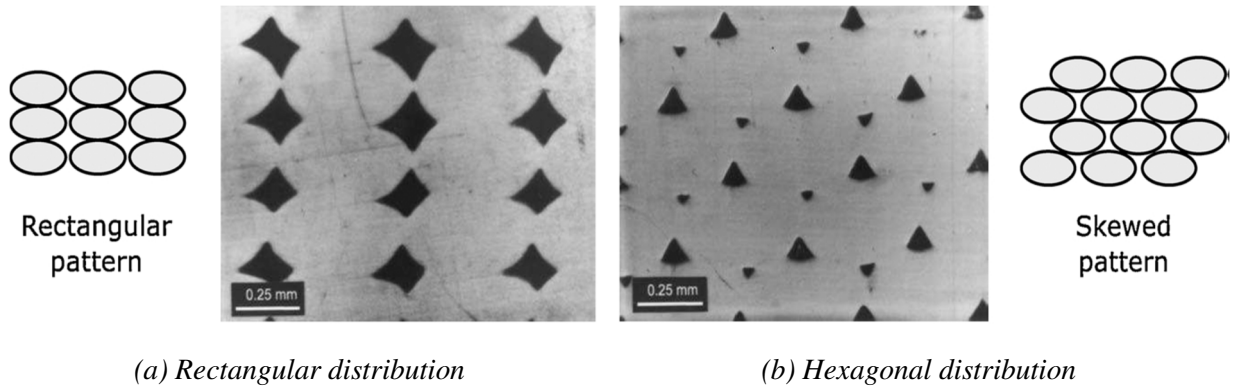
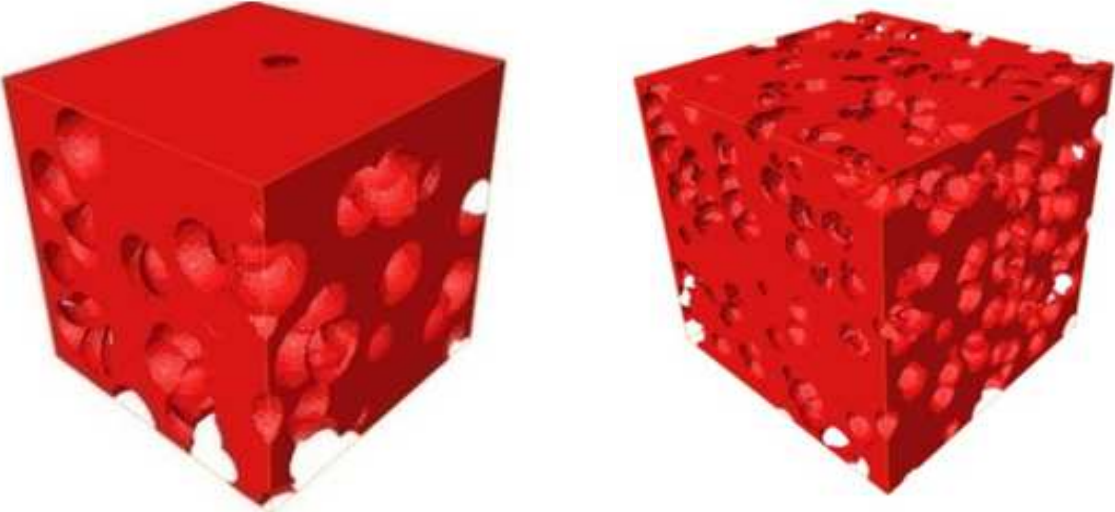


Figure 18: morphology of 3D printed polymers with different distributions of pores [165].

In this section, the Poisson process was used to create the RVE with a random distribution of the pores. By using this process, pores are consecutively added into the matrix of the RVE by randomly generated coordinate center, and then it is checked to avoid the overlap scheme for the hard model or with intersection for the case of Boolean model. The repulsion distance, or the minimum distance between two neighboring pores, is defined in the algorithm in order to create an adequate finite element mesh. Not that, the contour of pores is not very close to boundaries of RVE in order to avoid the occurrence of distorted finite elements. Therefore, the pore is accepted only when the center distance between the i th pores and other pores accepted previously has not exceed the minimum distance and the fixed volume fraction. Using the Poisson process, it is not possible to create a volume fraction up to 28% without overlapping of pores. The microstructure is controlled by three principal morphological parameters as: pore volume fractions, number and size of pores. Figure 19 shows an example

of porous polymers created with the Poisson process. These RVEs can be used for numerical modeling of mechanical properties of 3D printed composites.



(b) Lower density of pores

(b) Higher density of pores

Figure 19: RVEs of 3D printed polymer composites generated with a Poisson process based a random distribution of pores.

For example, in an FDM process, the polymer was heated up to the melt state and then extruded through a nozzle. The extruded polymer is then deposited on the previous layer as shown in Figure 20, creating a uniform distribution of pores trough 3D printing polymers. For the case of uniform distribution of pores, different RVEs are possible namely; square arrangement and hexagonal arrangement. There are two configurations for the square RVE: (1) square RVE with four pores at the corners and one pore at the middle and (2) square RVE with four pores at the corners. For the hexagonal arrangement, six pores are placed at the corners of the hexagon RVE and one single pore is placed at the middle of the RVE.

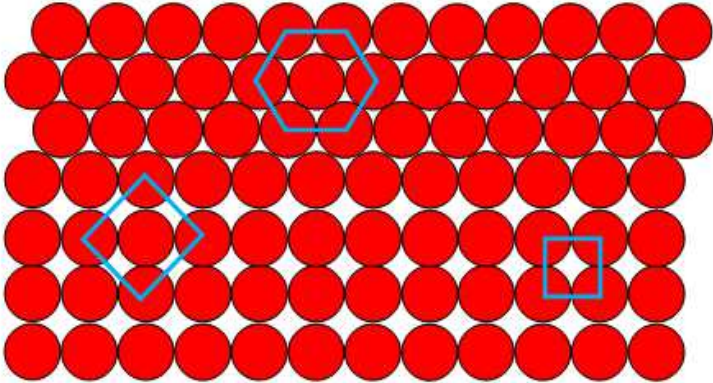


Figure 20: Different RVEs possibilities for the case of the uniform distribution of pores.

The generated RVEs by Poisson process can be used in order to model the effect of pores on the mechanical properties of 3D printed polymer composites. Analysis of the SEM microstructures of 3D printed polymer composites at different temperatures shows that the increasing flow liquid polymer with increasing the temperature changes the form and the distribution of created pores and voids. The interlayer boundaries of composites are still weakened due to the formation of pores during the process. Figure 21 shows an example of the SEM microstructure for 210°C and 250°C. From these images, voids on specimens made at elevated temperature have smaller areas. For this reason, the increase in the temperature during the printing process leads to an increase of the strength with the diminution of the pore volume in printed polymers. At 250°C the mechanical properties increases due to an increase in the cohesion surface between layers of composites.

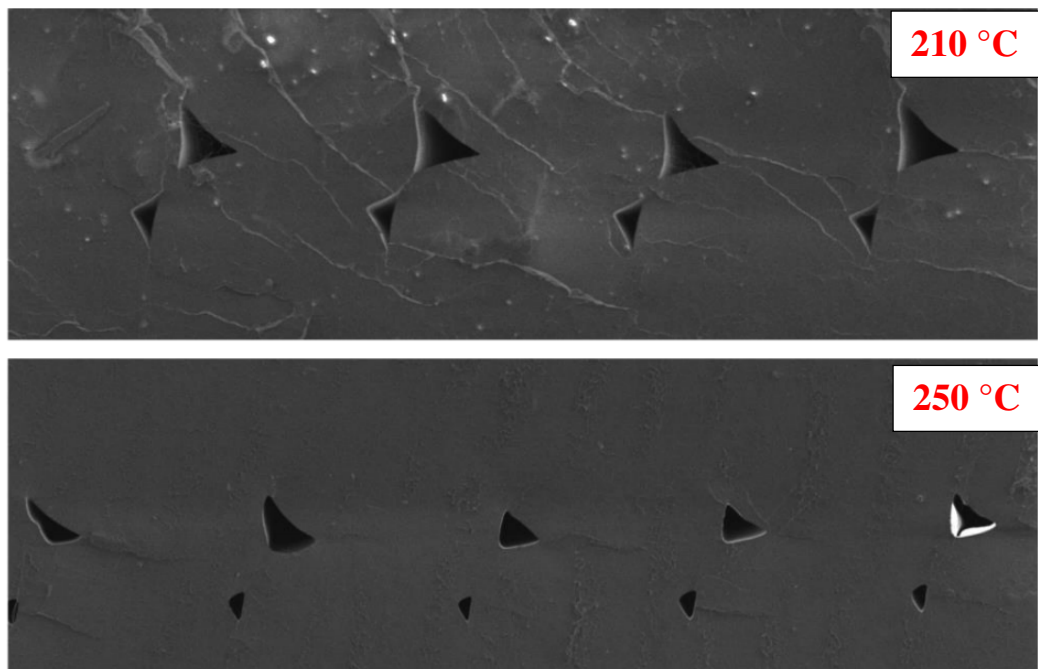
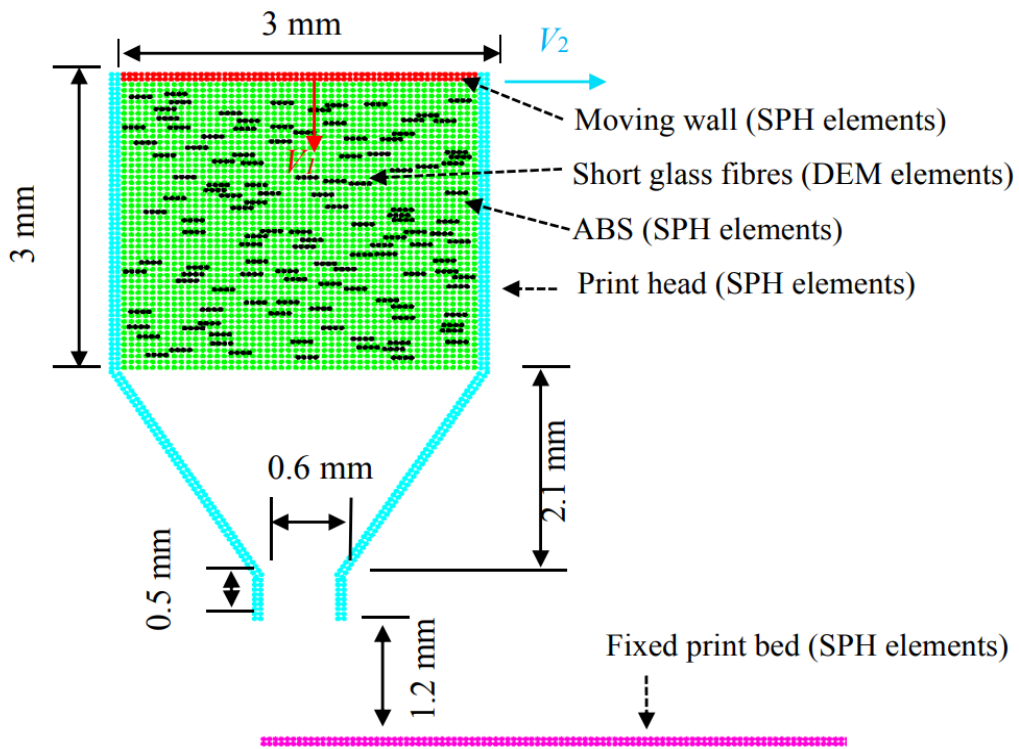


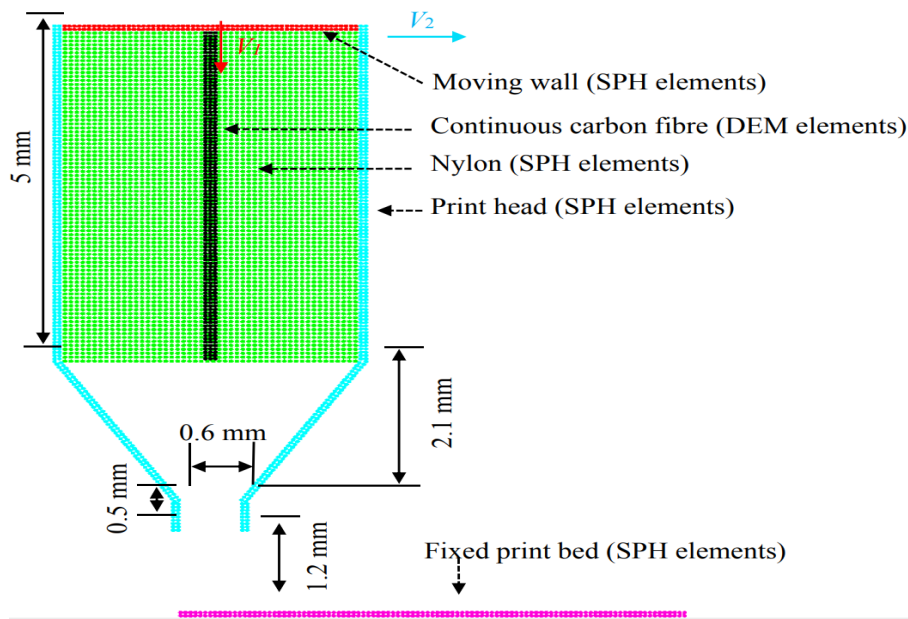
Figure 21: Distribution of the pore in 3D printed polymer composites at different temperatures [166].

Owing to their ability to print different complex shapes of composites, it is of great interest to use the numerical model, with the help of simulation software, in order to simulate the effect of parameters process on the mechanical properties of 3D printed composites. Despite the potential applications of 3D printed polymer composites, numerical simulation on such processes and materials are essentially nonexistent. No scientific studies were found on the open literature concerning this area. Edited by Hannah Mason [167] on 11/14/2018, an AM process simulation tool for predicting the concentration of stress and the distortion of the

specimens during the printing process will be launched with January 2019. This software uses a digital twin to simulate the effect of process parameters and automatically generating the corrected part to compensate the distortions. A new numerical technique for modeling the AM process of fibers reinforced polymers using FDM process was presented in [168]. This approach was based on the coupling between SPH and DEM techniques. This approach demonstrates also its capability for modeling short and continuous fibers reinforced 3D printed polymer composites. Figure 22 shows a schematic representation of the simulation of printing processes as proposed in [168]. The dimension of the head and nozzle were given in the figure. The short fibers were randomly oriented and distributed parallel to the wall, while the continuous fibers were positioned at the center of the print head perpendicular to the wall. The printing speed of 400 mm/s was used. In figure 23, it can be seen that the distribution of fibers becomes random. In the zones where the fibers are close to the walls, the velocity of the polymers is noticeable due to the effect of boundary, therefore the orientation of fibers in these zones changes significantly and move parallel with wall boundary. In the middle of the printing head, the orientation of fibers changes slightly. For example, in order to simulate FDM process for improving the mechanical properties, the process and the quality of 3D printed composites, a thorough understanding of the technique is essential. Figure 24 shows the important physical phenomena which are considered in the numerical model of 3D printing process. The representative geometry of the nozzle of FDM process and its dimension are given in Figure 25.



(a) Short fibers reinforced polymer composites



(b) Long fibers reinforced polymer composites

Figure 22: Initial configuration for the 3D printing process of polymer composites [168].

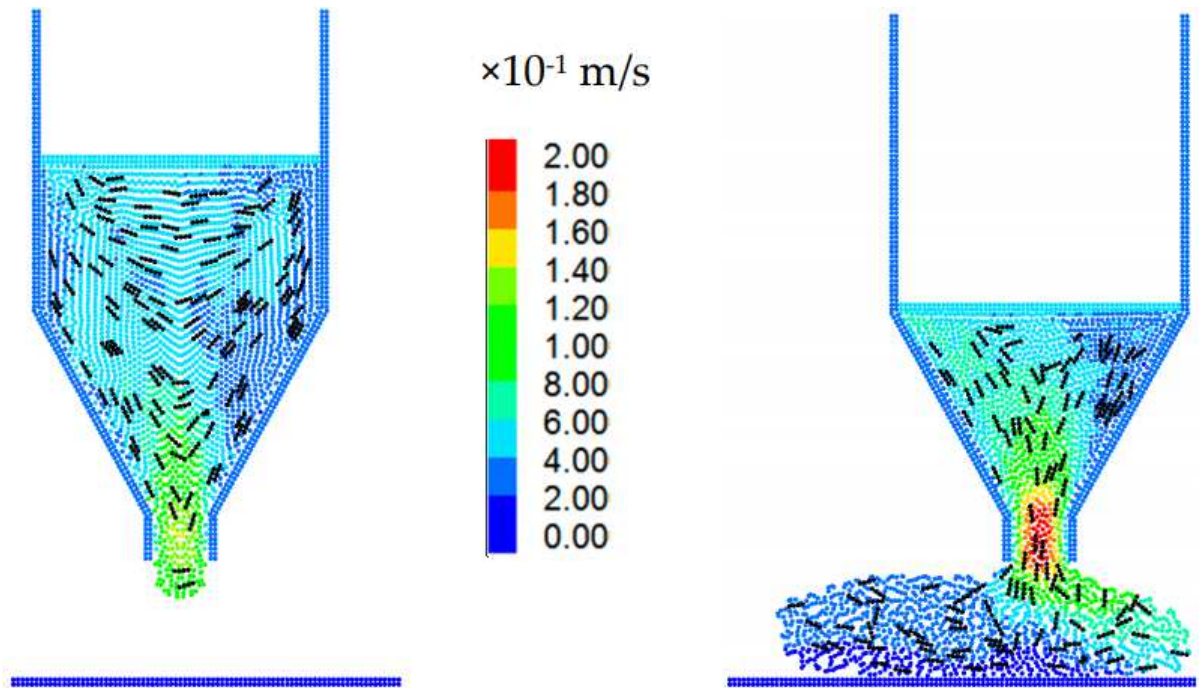


Figure 23: Distribution of the fibers during 3D printing process and velocities of polymers [168].

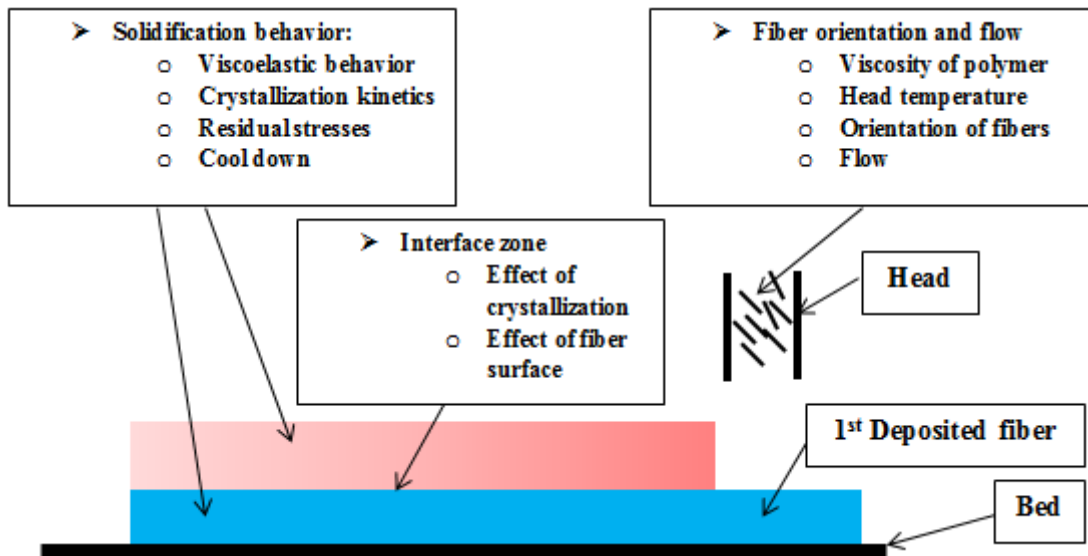


Figure 24: Physical phenomena associated with the simulation of FDM process.

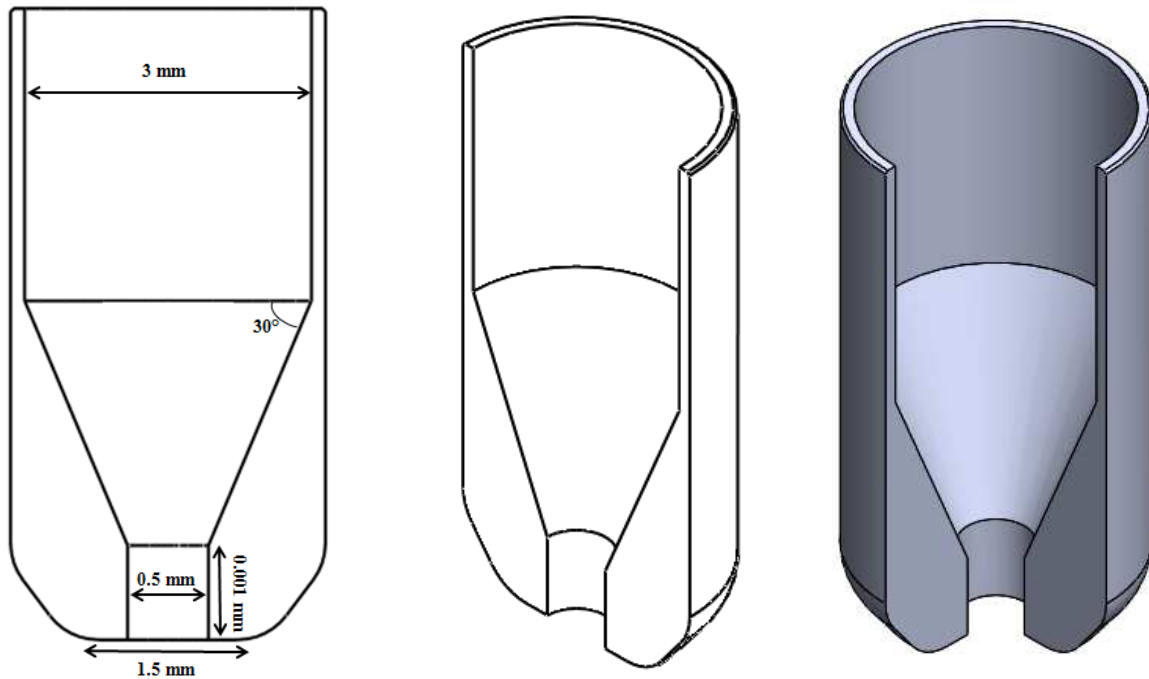


Figure 25: Geometry of the nozzle for the simulation of FDM process.

In addition to the formation of voids during 3D printing of polymers, and the complexity to simulate the 3D printing process, other several limitations need to be overcome and challenged at all levels:

- Machine level: existing machines are too slow and limited. It is difficult to print large parts. New 3D printing techniques with fast processing of composites should be developed. Another limitation concerns the feedback machines, i.e., if an error occurs during printing of composites, the process needs to be stopped, causing the waste of materials and time. A built-in feedback system should be developed. Calibrating of the 3D printing machine is still a quite complex task and requires proper training with a dedicated staff.
- Materials: Selected polymers for 3D printing of composites are limited. Only, thermoplastic polymer with a low glass transition temperature and appropriate melting viscosity could be used. The future effort might need to be focused on the possibility of using other polymers. Bio-polymers with medical applications need also to be developed in order to reduce the environmental impact. These techniques have a great promise in the printing of 3D tissues. Only a few of bio-printed tissues have achieved. Many challenges need to be overcome in this area.
- Performance: the objective of 3D printing was the fabrication of the composites with excellent properties compared with polymer composites manufactured by the

traditional process, but most of the printed composites still have a low mechanical strength. A main factor for the reduction of the mechanical properties is the presence of voids in printed parts and their molecular orientation. The percentage of porosity increase with the addition of reinforcement because of poor interfacial bonding with the polymer. Therefore, the efforts can focus on the elimination of voids during printing and ensure good interfacial bonding between the reinforcement phase and the polymer.

- **Advanced Modelling:** traditionally, the characterization and the modelling of 3D printed polymer composites focus on different length scales. This requires a multiscale analysis that is based on the fundamental laws of nature and links the electronic structure through the atomistic and mesoscale length to the macroscopic material behavior. Figures 26 and 27 show some examples demonstrating the scale analysis of the polymer composites. In each scale, a number of different physical phenomena are considered for the characterization of the printed part. For example, on the atomistic nanometer scale this is the molecular dynamics technique that introduces the polymer atoms interaction and move and their effect on the mechanical properties. Molecular dynamic simulation of 3D printed polymers provides a fundamental view on part deformation describing the fracture mode, diffusion and other physical mechanisms cannot be reached by experimental techniques. The concept is to calculate the dynamic trajectory of each atom by considering their interaction potentials and solving the equation of motion. The chemical and structural properties of atoms affect the properties of 3D printed polymers [169-171]. The role of the molecular modeling of 3D printed polymers is to enable engineering design at the component and systems application.

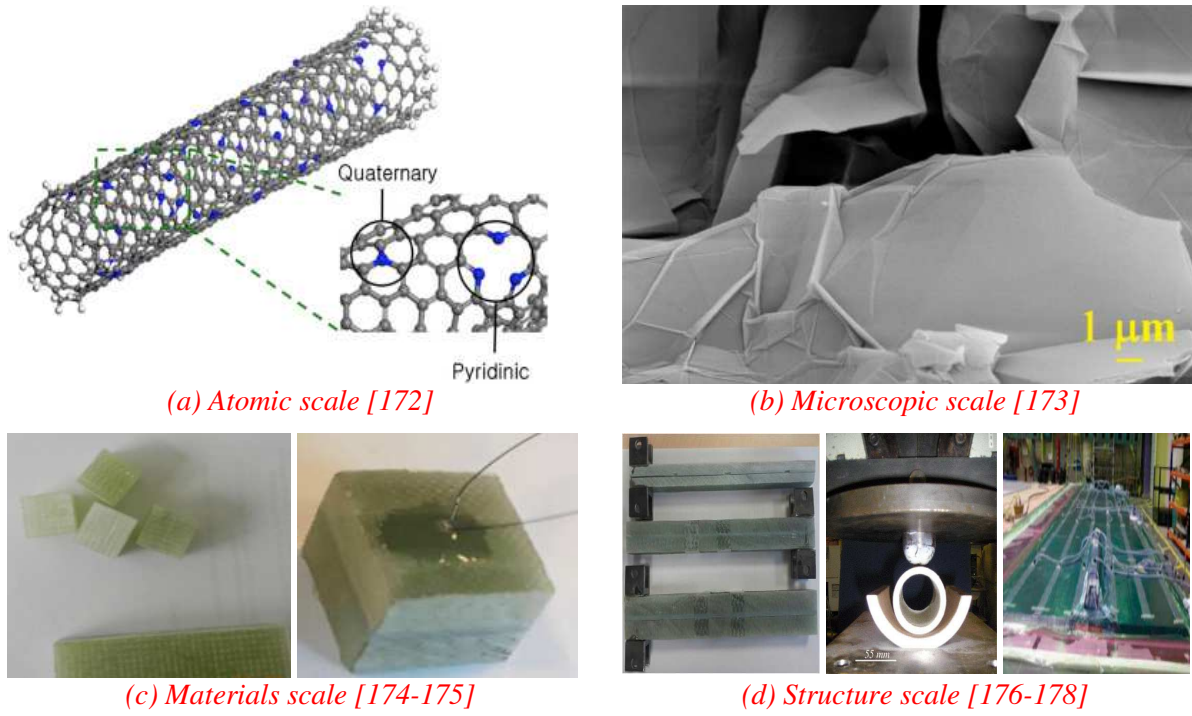


Figure 26: Different scales of polymer composites.

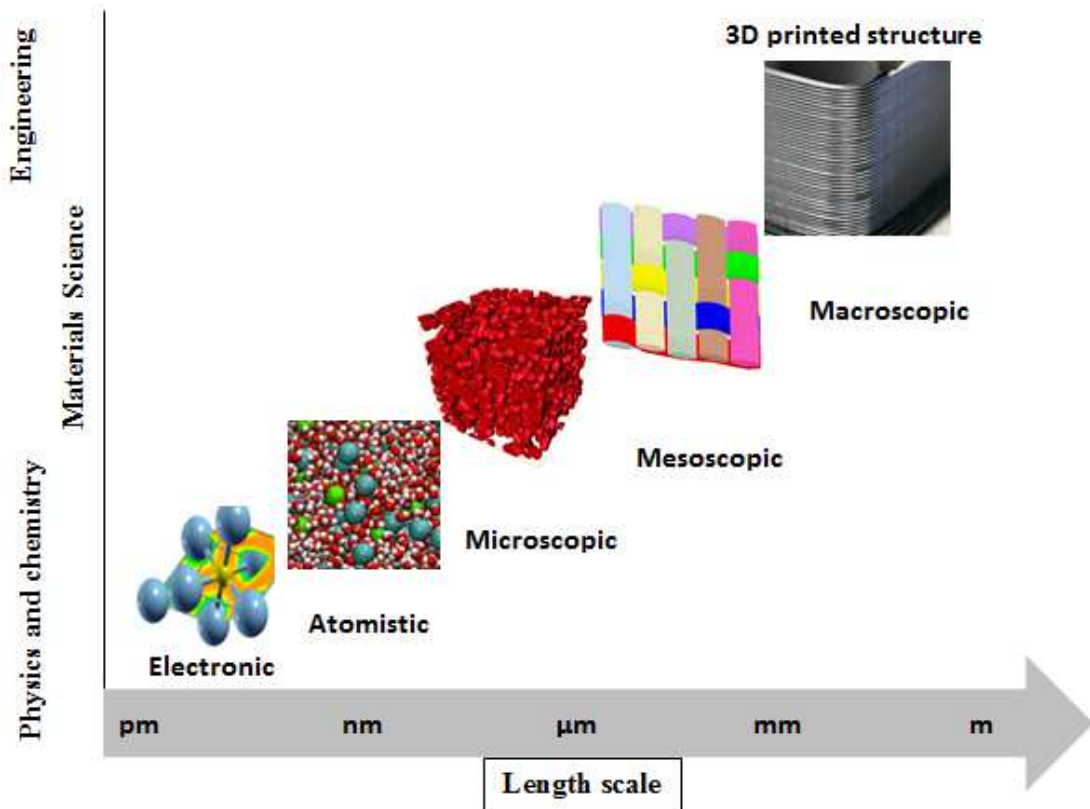


Figure 27: Hierarchical modeling of 3D printed composites.

- **Advanced fields:** the efforts of additive manufacturing can be conducted on the sensing field with different applications in medical and aeronautic structures. It consists to implant sensors within structure, using AM, in order to analyze the data change during operational conditions. The majority of the conventional actuators were fabricated using multistep manual fabrications with a less flexibility in the reproducibility of final products. Using AM, the sensing element is embedded within printed part and it can be used to sense different types of physical loads like force and deformations. Various investigations have been discussed the implantation of sensors into traditional structures [179-180], but the used of AM remains a challenge. 3D printed polymer composites are able to function as electronic components and an example was fabricated by Simon et al. [181] through FDM printing of carbon black reinforced PCL polymers. Similarly, the 3D printing of CNT reinforced epoxy has also been studied for various applications in printed electronic components [182]. Utilizing this nanocomposites, a sensor with a high electromechanical sensitivity was realized (gauge factor of 22). These functional sensors demonstrated the promising application of 3D printing technology on electronic devices. The embedding of a sensor allows an end user the ability to monitor specific critical regions. AM techniques print material layer by layer, thus have a great potential to accelerate process by embedding actuators into specimens. Clearly, this point deserves further study.

Despite numerous limitations, 3D printing technology is developing in a fast paste. This development was proven by numerous published articles and various printed parts in medical, aeronautics, electronics, automotive and other fields. 3D printers are not yet capable to manage the volumes required by the industrial demands. This technique must evolve further in order to outmatch some traditional manufacturing process. This paper presents a way for which further researchers will investigate more, in terms of materials, process and the performance of the product.

Acknowledgments: This work was funded by DGA France (Direction générale de l'armement - Ministry of Defense), MRIS program. The Authors of this paper gratefully acknowledge the financial support of the DGA, France.

References

- [1] Standard A. F2792, Standard Terminology for Additive Manufacturing Technologies. West Conshohocken, Pa, USA: ASTM International; 2012.
- [2] Hull, C.W., Apparatus for production of three-dimensional objects by stereolithography. 1986, Google Patents.
- [3] Huang S, Liu P, Mokasdar A, Hou L. Additive manufacturing and its societal impact: a literature review, *Int J Adv Manuf Technol* 67; 2013:1191–1203. DOI 10.1007/s00170-012-4558-5.
- [4] Bose S, Ke D, Sahasrabudhe H, Bandyopadhyay A. Additive manufacturing of biomaterials, *Progress in Materials Science* 93; 2018: 45–111.
- [5] Mokasdar A. A Quantitative Study of the Impact of Additive Manufacturing in the Aircraft Spare Parts Supply Chain, University of Cincinnati, 2012.
- [6] Michaels K. Aerospace's next disruptive technology; Additive manufacturing holds huge implications for OEMs, suppliers and the workforce, *Aviation Week & Space Technology*, 2013.
- [7] Coykendall J, Cotteleer M, Holdowsky J, Mahto M. 3D opportunity in aerospace and defense: additive manufacturing takes flight. A Deloitte series on additive manufacturing. Deloitte University Press; 2015. On- line http://d2mtr37y39tpbu.cloudfront.net/wp-content/uploads/2014/05/DUP_706-3D-Opportunity-Aerospace-Defense_MASTER2.pdf accessed 20.04.15 .
- [8] NASA. Space station 3-d printer builds ratchet wrench to complete first phase of operations, 2015, Online. accessed 21.03.15 http://www.nasa.gov/mission_pages/station/research/news/3Dratchet_wrench/ .
- [9] Ventola CL. Medical applications for 3D printing: current and projected uses, *Pharm. Therap*, 39; 2014: 704–711.
- [10] Giffi CA, Gangula B, Illinda P. 3D Opportunity in the Automotive Industry. *Additive Manufacturing Hits the Road*, Deloitte University Press, 2014, p.24.
- [11] Gibson I, Kvan T, Ming LW. Rapid prototyping for architectural models, *Rapid Prototyp. J*, 8; 2002: 91–99.
- [12] Lipton JI, Cutler M, Nigi F, Cohen D, Lipson H. Additive manufacturing for the food industry, *Trends Food Sci. Technol*, 43; 2015: 114–123.
- [13] Berman B. 3-D printing: The new industrial revolution, *Business Horizons*, 55, 2012; 155—162.
- [14] Crump SS. Fast, precise, safe prototype with FDM. *ASME, PED*, 50; 1991: 53–60.
- [15] Sood AK, Ohdar R, Mahapatra S. Parametric appraisal of mechanical property of fused deposition modelling processed parts, *Mater Des*, 31, 2010: 287e95.

- [16] Chacón JM, Caminero MA, García-Plaza E, Núñez PJ. Additive manufacturing of PLA structures using fused deposition modelling: Effect of process parameters on mechanical properties and their optimal selection, *Materials and Design*, 124; 2017: 143–157.
- [17] Chohan JS, Singh R, Boparai KS, Penna R, Fraternali F. Dimensional accuracy analysis of coupled fused deposition modeling and vapour smoothing operations for biomedical applications, *Compos B Eng*, 117; 2017: 138–49.
- [18] Mohamed OA, Masood SH, Bhowmik JL. Optimization of fused deposition modeling process parameters: a review of current research and future prospects. *Adv Manuf*, 3; 2015: 42–53.
- [19] Skelton J. Fused deposition modeling. *3D Printers and 3DPrinting Technologies Almanac*. <http://3d-print.blogspot.com/2008/02/fused-deposition-modelling.html>. Accessed 01 Aug 2012.
- [20] Tian X, Liu T, Yang C, Wang Q, Li D. Interface and performance of 3D printed continuous carbon fiber reinforced PLA composites, *Compos A Appl Sci Manuf*, 88; 2016: 198-205.
- [21] Le HP. Progress and trends in ink-jet print technology, *J Imaging Sci Techn*, 42, 1998: 49–62.
- [22] Sachs EM, Haggerty JS, Cima MJ, Williams PA. Three-dimensional printing techniques, 1993, Google Patents.
- [23] Perelaer J, et al. Printed electronics: The challenges involved in printing devices, interconnects, and contacts based on inorganic materials, *J. Mater. Chem.*, 20; 2010: 8446–8453.
- [24] Derby B. Printing and prototyping of tissues and scaffolds, *Science*, 338; 2012: 921–926.
- [25] Ngo TD, Kashani A, Imbalzano, Nguyen K, Hui D. Additive manufacturing (3D printing): A review of materials, methods, applications and challenges, *Composites Part B*, 143; 2018: 172–196.
- [26] Seerden KAM, Reis N, Evans JRG, Grant PS, Halloran JW, Derby B. Inkjet printing of wax-based alumina suspensions, *J. Am. Ceram. Soc.*, 84; 2001: 2514–2520.
- [27] Brian Derby. Additive Manufacture of Ceramics Components by Inkjet Printing. *Engineering* 2015, 1(1): 113–123. DOI 10.15302/J-ENG-2015014.
- [28] Hull C. Stereolithography: plastic prototype from CAD data without tooling, *Mod Cast*, 78; 1988.
- [29] Karalekas D, Antoniou K. Composite rapid prototyping: overcoming the drawback of poor mechanical properties, *J Mater Process Technol*, 153–154; 2004: 526–530.
- [30] Anderson J. Advantages and disadvantages of laser stereolithography. *Ezin Articles*. <http://ezinearticles.com/?Advantagesand-Disadvantages-of-Laser-Stereolithography&id04051331>. Accessed 03 Aug 2012.

[31] Travitzky N, Bonet A, Dermeik B, Fey T, Filbert-Demut I, Schlier L, Schlordt T, Greil P. Additive manufacturing of ceramic-based materials, *Adv Eng Mater*, 16; 2014: 729–754.

[32] Eckel ZC, Zhou C, Martin JH, Jacobsen AJ, Carter WB, Schaedler TA. Additive manufacturing of polymer-derived ceramics, *Science*, 351; 2016: 58–62.

[33] Wang X, Jiang M, Zhou Z, Gou J, Hui D. 3D printing of polymer matrix composites: a review and prospective, *Compos B Eng*, 110; 2017: 442–458.

[34] <https://3space.com/services/3d-printing/sla/>

[35] Beaman JJ, Barlow JW, Bourell DL, Crawford RH, Marcus HL, McAlea KP. *Solid freeform fabrication: a new direction in manufacturing*, Springer, 1996; New York

[36] Deckard C, Beaman JJ. Process and control issues in selective laser sintering, *ASME, PED*, 33; 1988, 33: 191–197.

[37] Gu D, Meiners W, Wissenbach K, Poprawe R. Laser additive manufacturing of metallic components: materials, processes and mechanisms, *Int Mater Rev*, 57; 2012: 133–164.

[38] Goodridge R, Shofner M, Hague R, McClelland M, Schlea M, Johnson R, Tuck C. Processing of a Polyamide-12/carbon nanofibre composite by laser sintering, *Polym Test*, 30; 2011: 94–100.

[39] Bai J, Goodridge RD, Hague RJM, Song M. Improving the mechanical properties of laser-sintered polyamide 12 through incorporation of carbon nanotubes, *Polym Eng Sci*, 53; 2013: 1937–1946.

[40] Salmoria GV, Paggi RA, Lago A, Beal VE. Microstructural and mechanical characterization of PA12/MWCNTs nanocomposite manufactured by selective laser sintering, *Polym Testing*, 30; 2011: 611–615.

[41] Goodridge RD, Shofner ML, Hague RJM, McClelland M, Schlea MR, Johnson RB, et al. Processing of a Polyamide-12/carbon nanofibre composite by laser sintering. *Polym Testing*, 30; 2011: 94–100.

[42] Rimell JT, Marquis PM. Selective laser sintering of ultra high molecular weight polyethylene for clinical applications, *J Biomed Mater Res*, 53; 2000: 414–420.

[43] Salmoria GV, Ahrens CH, Klaus P, Paggi RA, Oliveira RG, Lago A. Rapid manufacturing of polyethylene parts with controlled pore size gradients using selective laser sintering, *Mater Res*, 10; 2007: 211–214.

[44] Kruth JP, Levy G, Klocke F, Childs T. Consolidation phenomena in laser and powder-bed based layered manufacturing, *CIRP Ann – Manuf Technol*, 56; 2007: 730–759.

[45] Williams JM, Adewunmi A, Schek RM, Flanagan CL, Krebsbach PH, Feinberg SE, et al. Bone tissue engineering using polycaprolactone scaffolds fabricated via selective laser sintering, *Biomaterials*, 26; 2005: 4817–4827.

[46] Schmidt M, Pohle D, Rechtenwald T. Selective laser sintering of PEEK. *CIRP Ann – Manuf Technol*, 56; 2007: 205–208.

[47] Shahzad K, Deckers J, Zhang Z, Kruth J-P, Vleugels J. Additive manufacturing of zirconia parts by indirect selective laser sintering, *J Eur Ceram Soc*, 34; 2014: 81–89.

[48] Formlabs company. An Introductory Guide to SLS 3D Printing. <https://formlabs.com/blog/what-is-selective-laser-sintering/>

[49] 3DSourced. Selective Laser Sintering: Everything You Need To Know About SLS 3D Printing. <https://3dsourced.com/3d-printing-technologies/selective-laser-sintering-sls/>

[50] Gu DD, Meiners W, Wissenbach K, Poprawe R. Laser additive manufacturing of metallic components: materials, processes and mechanisms, *Int Mater Rev*, 57; 2012: 133–164.

[51] Goodridge RD, Tuck CJ, Hague RJM. Laser sintering of polyamides and other polymers, *Progress in Materials Science*, 57; 2012: 229-267.

Hofmann M. 3D printing gets a boost and opportunities with polymer materials, *ACS Macro Lett*, 3; 2014: 382–386.

[52] Tymrak B, Kreiger M, Pearce J. Mechanical properties of components fabricated with open-source 3-D printers under realistic environmental conditions, *Mater Des* 58; 2014: 242-246.

[53] Sun Q, Rizvi G, Bellehumeur C, Gu P. Effect of processing conditions on the bonding quality of FDM polymer filaments, *Rapid Prototyp J*, 14; 2008: 72-80.

[54] Tran P, Ngo TD, Ghazlan A, Hui D. Bimaterial 3D printing and numerical analysis of bio-inspired composite structures under in-plane and transverse loadings. *Compos Part B: Eng*, 108; 2017: 210-223.

[55] Melnikova R, Ehrmann A, Finsterbusch K. 3D printing of textile-based structures by Fused Deposition Modelling (FDM) with different polymer materials, *IOP Conference series: Materials science and engineering*, 62; 2014: 12-18.

[56] Dou J, Zhang Q, Ma M, Gu J. Fast fabrication of epoxy-functionalized magnetic polymer core-shell microspheres using glycidyl methacrylate as monomer via photo-initiated miniemulsion polymerization, *J Magnetism Magnetic Mater*, 324; 2012: 3078-3082.

[57] Ngoa TD, Kashania A, Imbalzano G, Nguyena KTQ, Hui D. Additive manufacturing (3D printing): A review of materials, methods, applications and challenges, *Composites Part B* 143; 2018: 172–196.

[58] Parandoush P, Lin D. A review on additive manufacturing of polymer-fiber composites, *Composite Structures*, 182; 2017: 36–53.

[59] Carneiro O, Silva A, Gomes R. Fused deposition modeling with polypropylene, *Mater Des*, 83; 2015: 768–776.

[60] Shofner ML, Lozano K, Rodríguez-Macías FJ, Barrera EV. Nanofiber-reinforced polymers prepared by fused deposition modeling, *J Appl Polym Sci*, 89; 2003: 3081–3090.

[61] Chung H, Das S. Processing and properties of glass bead particulate-filled functionally graded Nylon-11 composites produced by selective laser sintering, *Mater Sci Eng A*, 437; 2006: 226-234.

- [62] Nikzad M, Masood S, Sbarski I. Thermo-mechanical properties of a highly filled polymeric composites for fused deposition modeling, *Mater Des*, 32; 2011: 3448-3456.
- [63] Boparai K, Singh R, Singh H. Comparison of tribological behaviour for Nylon6-Al₂O₃ and ABS parts fabricated by fused deposition modelling: this paper reports a low cost composite material that is more wear-resistant than conventional ABS, *Virtual Phys Prototyp*, 10; 2015: 59-66.
- [64] Isakov D, Lei Q, Castles F, Stevens C, Grovenor C, Grant P. 3D printed anisotropic dielectric composite with meta-material features, *Mater Des*, 93; 2016: 423-430.
- [65] Shemelya CM, Rivera A, Perez AT, Rocha C, Liang M, Yu X, Kief C, Alexander D, Stegeman J, Xin H. Mechanical, Electromagnetic, and X-ray Shielding Characterization of a 3D Printable Tungstene Polycarbonate Polymer Matrix Composite for Space-Based Applications, *J Electron Mater*, 44; 2015: 2598-2607.
- [66] Boparai K, Singh R, Singh H. Comparison of tribological behaviour for Nylon6-Al₂O₃ and ABS parts fabricated by fused deposition modelling, *Virtual Phys Prototyp*, 10; 2015: 59-66.
- [67] Türk DA, Brenni F, Zogg M, Meboldt M. Mechanical characterization of 3D printed polymers for fiber reinforced polymers processing, *Materials and Design*, 118; 2017: 256–265.
- [68] Hao W, Liu Y, Zhou H, Chen H, Fang D. Preparation and characterization of 3D printed continuous carbon fiber reinforced thermosetting composites, *Polymer Testing*, 65; 2018: 29–34.
- [69] Ning F, Cong W, Qiu J, Wei J, Wang S. Additive manufacturing of carbon fiber reinforced thermoplastic composites using fused deposition modeling, *Compos B Eng*, 80; 2015: 369–378.
- [70] Tian X, Liu T, Yang C, Wang Q, Li D. Interface and performance of 3D printed continuous carbon fiber reinforced PLA composites, *Compos. Part A-Appl. S*, 88; 2016: 198–205.
- [71] Li N, Li Y, Liu S. Rapid prototyping of continuous carbon fiber reinforced polylactic acid composites by 3D printing, *J. Mat. Process Tech*, 238; 2016: 218–225.
- [72] Parandoush P, Lin D. A review on additive manufacturing of polymer-fiber composites, *Compos Structures*, 182; 2017: 36–53.
- [73] Tekinalp HL, Kunc V, Velez-Garcia GM, Duty CE, Love LJ, Naskar AK, Blue CA, Ozcan S. Highly oriented carbon fiber–polymer composites via additive manufacturing, *Compos Sci Technol*, 105; 2014: 144–150.
- [74] Bakarich SE, Gorkin III R, Panhuis MIH, Spinks GM. Three-dimensional printing fiber reinforced hydrogel composites, *ACS Appl Mater Interfaces*, 6; 2014: 15998–6006.
- [76] Kim E, Shin YJ. The effects of moisture and temperature on the mechanical properties of additive manufacturing components: fused deposition modeling, *Rapid Prototyp. J.*, 22; 2016: 887–894, <http://dx.doi.org/10.1108/RPJ-08-2015-0095>.

[77] Bagsik A, Schöppner V, Klemp E. FDM part quality manufactured with Ultem*9085, Proceedings of the 14th International Scientific Conference on Polymeric Materials: Halle (Saale), 2010.

[78] Masood SH, Song WQ. Development of new metal/polymer materials for rapid tooling using Fused deposition modelling, *Mater. Des.*, 25; 2004: 587–594, <http://dx.doi.org/10.1016/j.matdes.2004.02.009>.

[79] Nikzad M, Masood SH, Sbarski I. Thermo-mechanical properties of a highly filled polymeric composites for Fused Deposition Modeling, *Mater. Des.*, 32; 2011: 3448–3456.

[80] Kalsoom U, Peristyy A, Nesterenko P, Paull B. A 3D printable diamond polymer composite: a novel material for fabrication of low cost thermally conducting devices, *RSC Adv*, 6; 2016: 3814-3817.

[81] Hwang S, Reyes EI, Moon K-s, Rumpf RC, Kim NS. Thermo-mechanical Characterization of Metal/Polymer Composite Filaments and Printing Parameter Study for Fused Deposition Modeling in the 3D Printing Process, *J Electron Mater*, 44; 2015: 771-777.

[82] Fantino E, Chiappone A, Calignano F, Fontana M, Pirri F, Roppolo I. In Situ Thermal Generation of Silver Nanoparticles in 3D Printed Polymeric Structures, *Materials*, 9; 2016: 589. doi:10.3390/ma9070589.

[83] Chiappone A, Roppolo I, Naretto E, Fantino E, Calignano F, Sangermano M, Pirri F. Study of graphene oxide-based 3D printable composites: effect of the in situ reduction, *Compos B Eng*, 124; 2017: 9–15.

[84] Dul S, Fambri L, Pegoretti A. Fused deposition modelling with ABS–graphene nanocomposites, *Compos Appl Sci Manuf*, 85; 2016: 181–191.

[85] Han Y, Wang F, Wang H, Jiao X, Chen D. High-strength boehmite-acrylate composites for 3D printing: reinforced filler-matrix interactions, *Compos Sci Technol*, 154; 2018: 104–109.

[86] Chen Y, Mao J, Wu J. Microwave transparent crosslinked polystyrene nanocomposites with enhanced high voltage resistance via 3D printing bulk polymerization method, *Compos Sci Technol*, 157; 2018: 160–167.

[87] Postiglione G, Natale G, Griffini G, Levi M, Turri S. Conductive 3D microstructures by direct 3D printing of polymer/carbon nanotube nanocomposites via liquid deposition modeling, *Compos Appl Sci Manuf*, 76; 2015: 110–114.

[88] Weng Z, Zhou Y, Lin W, Senthil T, Wu L. Structure-property relationship of nano enhanced stereolithography resin for desktop SLA 3D printer, *Compos Appl Sci Manuf*, 88; 2016: 234–242.

[89] Boparai KS, Singh R, Fabbrocino F, Fraternali F. Thermal characterization of recycled polymer for additive manufacturing applications, *Compos B Eng*, 106; 2016: 42–47.

[90] Han Y, Wang F, Wang H, Jiao X, Chen D. High-strength boehmite-acrylate composites for 3D printing: reinforced filler-matrix interactions, *Compos Sci Technol*, 154; 2018: 104–109.

- [91] Billiet T, Gevaert E, De Schryver T, Cornelissen M, Dubruel P, *Biomaterials*, The 3D printing of gelatin methacrylamide cell-laden tissue-engineered constructs with high cell viability, 35; 2014: 49-62.
- [92] Billiet T, Gevaert E, De Schryver T, Cornelissen M, Dubruel P. *Biomaterials*. 2014; 35:49.
- [93] Griffith LG. *Polymeric biomaterials, Acta Materialia*, 48; 2000: 263-277.
- [94] Do AV, Khorsand B, Geary SM, Salem AK. 3D Printing of Scaffolds for Tissue Regeneration Applications, *Adv Healthc Mater*, 4; 2015: 1742–1762.
- [95] Korossis S, Bolland F, Southgate J, Ingham E, Fisher J, Regional biomechanical and histological characterisation of the passive porcine urinary bladder: Implications for augmentation and tissue engineering strategies, *Biomaterials*, 30; 2009: 266-275.
- [96] Groeber F, Holeiter M, Hampel M, Hinderer S, Schenke-Layland K. Skin tissue engineering--in vivo and in vitro applications, *Clin Plast Surg*, 39; 2012: 33-58.
- [97] Inzana JA, Olvera D, Fuller SM, Kelly JP, Graeve OA, Schwarz EM, Kates SL, Awad HA, *Biomaterials*, 35; 2014: 4026-4034.
- [98] Serra T, Planell JA, Navarro M. High-resolution PLA-based composite scaffolds via 3-D printing technology, *Acta Biomaterialia*, 9; 2013: 5521-55.
- [99] Kim J, McBride S, Tellis B, Alvarez-Urena P, Song Y-H, Dean DD, Sylvia VL, Elgandy H, Ong J, Hollinger JO. Rapid-prototyped PLGA/b-TCP/hydroxyapatite nanocomposite scaffolds in a rabbit femoral defect model, *Biofabrication*, 4; 2012: 025003.
- [100] Diogo G, Gaspar V, Serra I, Fradique R, Correia I. Manufacture of b-TCP/alginate scaffolds through a Fab@home model for application in bone tissue engineering, *Biofabrication*, 6; 2014: 025001.
- [101] Davila J, Freitas M, Inforçatti Neto P, Silveira Z, Silva J, d'Avila M. Fabrication of PCL/b-TCP scaffolds by 3D mini-screw extrusion printing, *J Appl Polym Sci*, 15; 2016: 43031.
- [102] Xia Y, Zhou P, Cheng X, Xie Y, Liang C, Li C, Xu S, Selective laser sintering fabrication of nano-hydroxyapatite/poly- ϵ -caprolactone scaffolds for bone tissue engineering applications, *Int J Nanomedicine*, 8; 2013: 4197-4213.
- [103] Jakus AE, Secor EB, Rutz AL, Jordan SW, Hersam MC, Shah RN. Threedimensional printing of high-content graphene scaffolds for electronic and biomedical applications, *ACS Nano*, 9; 2015: 4636-4648.
- [104] Lee H, Kim Y, Kim S, Kim G. Mineralized biomimetic collagen/alginate/silica composite scaffolds fabricated by a low-temperature bio-plotting process for hard tissue regeneration: fabrication, characterisation and in vitro cellular activities, *J Mater Chem B*, 2; 2014: 5785-5798.
- [105] Yildirim ED, Yin X, Nair K, Sun W. Fabrication, characterization, and biocompatibility of single-walled carbon nanotube-reinforced alginate composite scaffolds manufactured using freeform fabrication technique, *J Biomed Mater Res Part B Appl Biomaterials*, 87; 2008: 406-414.

- [106] Zhang J, Zhao S, Zhu M, Zhu Y, Zhang Y, Liu Z, Zhang C. 3D-printed magnetic Fe₃O₄/MBG/PCL composite scaffolds with multifunctionality of bone regeneration, local anticancer drug delivery and hyperthermia, *J Mater Chem B*, 2; 2014: 7583-7595.
- [107] Senatov F, Niaza K, Stepashkin A, Kaloshkin S. Low-cycle fatigue behavior of 3d-printed PLA-based porous scaffolds, *Compos Part B Eng*, 97; 2016: 193-200.
- [108] Bose S, Vahabzadeh S, Bandyopadhyay A. 3D Printed Scaffolds as a New Perspective for Bone Tissue Regeneration: Literature Review, *Materials Today*, 16; 2013: 496-504.
- [109] Perez ART, Roberson DA, Wicker RB. Fracture surface analysis of 3D-printed tensile specimens of novel ABS-based materials, *J Fail Analysis Prev*, 14; 2014: 343-353.
- [110] Wei X, Li D, Jiang W, Gu Z, Wang X, Zhang Z, Sun Z, 3D Printable Graphene Composite, *Scientific reports* 5; 2015.
- [111] Rymansaib Z, Iravani P, Emslie E, Medvidovic Kosanovic M, Sak Bosnar M, Verdejo R, Marken F. All Polystyrene 3D Printed Electrochemical Device with Embedded Carbon Nanofiber Graphite Polystyrene Composite Conductor, *Electroanalysis*, 28; 2016: 1517-1523.
- [112] Sandoval H, Wicker RB. Functionalizing stereolithography resins: effects of dispersed multi-walled carbon nanotubes on physical properties, *Rapid Prototyp J*, 12; 2006: 292-303.
- [113] Lin D, Jin S, Zhang F, Wang C, Wang Y, Zhou C, Cheng GJ. 3D stereolithography printing of graphene oxide reinforced complex architectures, *Nanotechnology*, 26; 2015: 434003.
- [114] Yugang D, Yuan Z, Yiping T, Dichen L. Nano-TiO₂-modified photosensitive resin for RP, *Rapid Prototyp J*, 17; 2011: 247-252.
- [115] Kim K, Zhu W, Qu X, Aaronson C, McCall WR, Chen S, Sirbuly DJ. 3D Optical Printing of Piezoelectric Nanoparticle-Polymer Composite Materials, *ACS Nano*, 8; 2014: 9799-9806.
- [116] Zhang Y, Li H, Yang X, Zhang T, Zhu K, Si W, Liu Z, Sun H. Additive manufacturing of carbon nanotube-photopolymer composite radar absorbing materials, *Polym Compos* 2016. <http://dx.doi.org/10.1002/pc.24117>.
- [117] He M, Zhao Y, Wang B, Xi Q, Zhou J, Liang Z. 3D Printing Fabrication of Amorphous Thermoelectric Materials with Ultralow Thermal Conductivity, *Small*, 11; 2015: 5889-5894.
- [118] Athreya SR, Kalaitzidou K, Das S. Processing and characterization of a carbon black-filled electrically conductive Nylon-12 nanocomposite produced by selective laser sintering, *Mater Sci Eng A*, 527; 2010: 2637-2642.
- [119] Zheng H, Zhang J, Lu S, Wang G, Xu Z. Effect of core-shell composite particles on the sintering behavior and properties of nano-Al₂O₃/polystyrene composite prepared by SLS, *Mater Lett*, 60; 2006: 1219-1223.

- [120] Chung H, Das S. Functionally graded Nylon-11/silica nanocomposites produced by selective laser sintering, *Mater Sci Eng A*, 487; 2008: 251-257.
- [121] Kutikov AB, Gurijala A, Song J. Rapid prototyping amphiphilic polymer/hydroxyapatite composite scaffolds with hydration-induced self-fixation behavior, *Tissue Eng Part C Methods*, 21; 2014: 229-241.
- [122] Voigt W. Ueber die Beziehung zwischen den beiden Elasticitätsconstanten isotroper Körper, *annalen der physic*, 1889. <https://doi.org/10.1002/andp.18892741206>.
- [123] Reuss A. Berechnung der Fließgrenze von Mischkristallen auf Grund der Plastizitätsbedingung für Einkristalle. *ZAMM—Journal of Applied Mathematics and Mechanics*, 9; 1929: 49-58. <http://dx.doi.org/10.1002/zamm.19290090104>
- [124] Hashin Z, Shtrikman S. A variational approach to the theory of the elastic behavior of multiphase materials, *Journal of the Mechanics and Physics of Solids*, 11: 1963: 127-140.
- [125] Beran M, Molyneux J. Use of classical variational principles to determine bounds for the effective bulk modulus in heterogeneous media, *Quarterly of Applied Mathematics*, 24: 1966; 107-118.
- [126] Milton GW. Bounds on the electromagnetic, elastic, and other properties of two component composites, *Physical Review Letters*, 46; 1981; 542.
- [127] Mori T, Tanaka K. Average stress in matrix and average elastic energy of materials with misfitting inclusions, *Acta metallurgica*, 21; 1973: 571-574.
- [128] Smallwood HM. Limiting law of the reinforcement of rubber, *Journal of applied physics*, 15; 1944: 758-766.
- [129] Guth E, Gold O. On the hydrodynamical theory of the viscosity of suspensions, *Phys. Rev*, 53; 1938: 2-15.
- [130] Torquato S. Random heterogeneous media: microstructure and improved bounds on effective properties, *Appl. Mech. Rev*, 44; 1991: 37-76.
- [131] Torquato S. Random heterogeneous media: Microstructure and improved bounds on effective properties, *Appl Mech Rev*, 44; 1991.
- [132] Christensen RM. A critical evaluation for a class of micromechanics models, *Journal of Mechanics and Physics of Solids*; 38; 1990: 379–404.
- [133] Matsuzaki R, et al. Three-dimensional printing of continuous-fiber composites by in-nozzle impregnation, *Scientific Reports*, 6; 2016: 23058. DOI: 10.1038/srep23058.
- [134] Halpin JC, Kardos JL. The Halpin-Tsai equations: A review, *Polymer Engineering and Science*, 16; 1976: 5.
- [135] Chamis CC. Mechanics of composite materials: past, present, and future, *J Compos Technol Res ASTM*, 11; 1989: 3–14.
- [136] Hashin Z, Rosen BW. The elastic moduli of fiber reinforced materials, *Journal of Applied Mechanics*, *Trans ASME*, 31; 1964: 223-232.
- [137] Barbero EJ. Introduction to composite materials design, CRC Press, 2010.

- [138] Adams DF. *Micromechanical Analysis of Composite Materials*, Technomic Publ., Lancaster, USA, 1989.
- [139] Bressan F, De Bona A, Soma` A. Design of composite laminates with low thermal expansion, *Proc. Instn Mech. Engrs, Part L: J. Materials: Design and Applications*. <https://doi.org/10.1177/146442070421800304>.
- [140] Melenka GW, Schofield JS, Dawson MR, Carey JP. Evaluation of dimensional accuracy and material properties of the MakerBot 3D desktop printer, *Rapid Prototyping J*, 21; 2015: 618–627.
- [141] Scida D, Aboura Z, Benzeggagha M, Bocherens E. A micromechanics model for 3D elasticity and failure of woven-fibre composite materials, *Composites Science and Technology*, 59; 1999: 505-517.
- [142] El Moumen A, Kanit T, Imad A, El Minor H. Computational thermal conductivity in porous materials using homogenization techniques: Numerical and statistical approaches, *Computational Materials Science*, 97; 2015: 148-158.
- [143] El Moumen A, Kanit T, Imad A, El Minor H. Effect of reinforcement shape on physical properties and representative volume element of particles-reinforced composites: Statistical and numerical approaches, *Mechanics of Materials*, 83; 2015: 1-16.
- [144] El Moumen A, Kanit T, Imad A, El Minor H. Effect of overlapping inclusions on effective elastic properties of composites, *Mechanics Research Communications*, 53; 2013: 24-30.
- [145] Kaddouri W, El Moumen A, Kanit T, Madani S, Imad A. On the effect of inclusion shape on effective thermal conductivity of heterogeneous materials, *Mechanics of Materials*, 92; 2016: 28-41.
- [146] El Moumen A, Imad A, Kanit T, Hilali E, El Minor H. A multiscale approach and microstructure design of the elastic composite behavior reinforced with natural particles, *Composites Part B: Engineering*, 66; 2014: 247-254.
- [147] Beicha D, Kanit T, Brunet Y, Imad A, El Moumen A, Khelfaoui Y. Effective transverse elastic properties of unidirectional fiber reinforced composites, *Mechanics of Materials*, 102; 2016: 47-53.
- [148] Bouaoune J, Brunet Y, El Moumen A, Kanit T, Mazouz H. Random versus periodic microstructures for elasticity of fibers reinforced composites, *Composites Part B: Engineering*, 103; 2016: 68-73.
- [149] Sukiman MS, Kanit T, N'Guyen F, Imad A, El Moumen A, Erchiqui F. Effective thermal and mechanical properties of randomly oriented short and long fiber composites, *Mechanics of Materials*, 107; 2017: 56-70.
- [150] El Moumen A, Tarfaoui M, Hassoon O, Lafdi K, Benyahia H, Nachtane M. Experimental study and numerical modelling of low velocity impact on laminated composite reinforced with thin film made of carbon nanotubes, *Applied Composite Materials*, 25; 2018; 25: 309–320.

- [151] Hassoon OH, Tarfaoui M, Alaoui AE, El Moumen A. Experimental and numerical investigation on the dynamic response of sandwich composite panels under hydrodynamic slamming loads, *Composite Structures*, 178; 2017: 297-307.
- [152] Hassoon OH, Tarfaoui M, El Moumen A. Progressive damage modeling in laminate composites under slamming impact water for naval applications, *Composite Structures*, 167; 2017: 178-190.
- [153] Erchiqui F, Souli M, Kanit T, Imad A, Boudlal A, El Moumen A. Characterization of polymeric membranes under large deformations using fluid-structure coupling, *International Journal of Applied Mechanics*, 7; 2015; 1550068.
- [154] El Moumen A, Tarfaoui M, Lafdi K. Computational Homogenization of Mechanical Properties for Laminate Composites Reinforced with Thin Film Made of Carbon Nanotubes, *Applied Composite Materials*, 25; 2018: 569–588.
- [155] Al Habis N, El Moumen A, Tarfaoui M, Lafdi K. Mechanical Properties of Carbon Black/Poly (ϵ -caprolactone)-Based Tissue Scaffolds, *Arabian Journal of Chemistry*. <https://doi.org/10.1016/j.arabjc.2018.10.005>.
- [156] Islam, M, Tudryn G, Picu C. Microstructure modeling of random composites with cylindrical inclusions having high volume fraction and broad aspect ratio distribution, *Computational Materials Science*, 125; 2016: 309–318.
- [157] Tashkinov M. Statistical methods for mechanical characterization of randomly reinforced media, *Mechanics of Advanced Materials and Modern Processes*, 3; 2017: DOI 10.1186/s40759-017-0032-2.
- [158] Ghossein E, Lévesque M. Homogenization models for predicting local field statistics in ellipsoidal particles reinforced composites: Comparisons and validations, *International Journal of Solids and Structures*, 58; 2015: 91–105.
- [159] Jean A, Jeulin D, Forest S, Cantournet S, N'guyen F. A multiscale microstructure model of carbon black distribution in rubber, *Journal of Microscopy*, 241; 2011: 243-260.
- [160] Zhang C, Curiel-Sosa JL, Duodu EA. Finite element analysis of the damage mechanism of 3D braided composites under high-velocity impact, *Journal of Materials Science*, 52; 2017: 4658-4674.
- [161] Panerai F, Ferguson J, Lachaud J, Martin A, Gasch M, Mansour N. Analysis of fibrous felts for flexible ablators using synchrotron hard x-ray micro-tomography, 8th European Symposium on Aerothermodynamics for Space Vehicles, 2015. <http://orioai.univ-nc.nc/search/notice.html?id=univ-nc.nc-ori-225312&printable=true>.
- [162] Cooke W, Tomlinson RA, Burguete R, Johns D, Vanard G. Anisotropy, homogeneity and ageing in an SLS polymer, *Rapid Prototyp J*, 17; 2011: 269–279.
- [163] Guessasma S, Belhabib S, Nouri H, Ben Hassana O. Anisotropic damage inferred to 3D printed polymers using fused deposition modelling and subject to severe compression, *Eur Polym J*, 85; 2016: 324–340.
- [164] Mühler T, Gomes CM, Heinrich J, Günster J. Slurry-based additive manufacturing of ceramics, *Int J Appl Ceram Technol*, 12; 2015: 18–25.

[165] Rodriguez JF, Thomas JP, Renaud JE. Characterization of the Mesostructure of Fused-Deposition Acrylonitrile-Butadiene-Styrene Materials, *Rapid Prototyping Journal*, 6; 2000: 175-185.

[166] Kuznetsov VE, Solonin AN, Tavitov AG, Urzhumtsev OD, Vakulik AH. Increasing of strength of FDM (FFF) 3D printed parts by influencing on temperature-related parameters of the process, *Preprints 2018*, Doi:10.20944/preprints201803.0102.v2.

[167] <https://www.compositesworld.com/products/siemens-announces-additive-manufacturing-software-tool-to-improve-3d-printing-accuracy>

[168] Yang D, Wu K, Wan L, Sheng Y. A Particle Element Approach for Modelling the 3D Printing Process of Fibre Reinforced Polymer Composites, *J. Manuf. Mater. Process*, 1; 2017. Doi:10.3390/jmmp1010010.

[169] Naddeo C, Vertuccio L, Barra G, Guadagno L. Nano-Charged Polypropylene Application: Realistic Perspectives for Enhancing Durability. *Materials* 10; 20107: 943. doi: 10.3390/ma10080943.

[170] Barra G, De Nicola F, De Vivo B, Egiziano L, Guadagno L, Lamberti P, Raimondo M, Spinelli G, Tucci V, Vertuccio, L, Vietri U, Volponi R. Enhanced electrical properties of carbon fiber reinforced composites obtained by an effective infusion process. 2014 IEEE 9th Nanotechnology Materials and Devices Conference, NMDC 2014. 23 December 2014, Article number 6997429, Pages 88-91.

[171] Raimondo M, Guadagno L, Vertuccio L, Naddeo C, Barra G, Spinelli G, Lamberti P, Tucci V, Lafdi K. Electrical conductivity of carbon nanofiber reinforced resins: Potentiality of Tunneling Atomic Force Microscopy (TUNA) technique. *Composites Part B: Engineering* 143; 2018: 148-160.

[172] Park C, Jung J, Yun G. Thermomechanical properties of mineralized nitrogen-doped carbon nanotube/polymer nanocomposites by molecular dynamics simulations. *Composites Part B: Engineering*, 161; 639-650.

[173] Tarfaoui M, Lafdi K, Beloufa I, Daloia D, Muhsan A. Effect of Graphene Nano-Additives on the Local Mechanical Behavior of Derived Polymer Nanocomposites. *Polymers* 10; 2018: 667. <https://doi.org/10.3390/polym10060667>

[174] Tarfaoui M, El Moumen A, Ben Yahia H. Damage detection versus heat dissipation in E-glass/Epoxy laminated composites under dynamic compression at high strain rate. *Composite Structures*, 186; 2018: 50-61.

[175] Sassi S, Tarfaoui M, Ben Yahia H. In-situ heat dissipation monitoring in adhesively bonded composite joints under dynamic compression loading using SHPB. *Composites Part B: Engineering* 154; 2018: 64-76.

[176] Shah OR, Tarfaoui M. Effect of adhesive thickness on the Mode I and II strain energy release rates. Comparative study between different approaches for the calculation of Mode I & II SERR's. *Composites Part B: Engineering* 96; 2016: 354-363.

[177] Gning PB, Tarfaoui M, Collombet F, Riouc L, Davies P. Damage development in thick composite tubes under impact loading and influence on implosion pressure: experimental observations. *Composites Part B: Engineering* 36; 2005: 306-318.

[178] Tarfaoui M, El Moumen A. Dynamic behavior of top-hat bonded stiffened composite panels: Experimental characterization. *Composites Part B: Engineering* 149; 2018: 216-226.

[179] Qureshi Y, Tarfaoui M, Lafdi KI, Lafdi K. Nanotechnology and Development of Strain Sensor for Damage Detection. In book: *Advances in Structural Health Monitoring*. DOI: 10.5772/intechopen.82871.

[180] De Baere D, Hinderdael M, Moonens M, Jardon Z, Lison M, Strantza M, Guillaume P. Additive Manufactured Metallic Smart Structures to Monitor the Mechanical Behavior In Situ. *Proceedings 2*; 2018: 500. doi:10.3390/ICEM18-05425.

[181] Leigh SJ, Bradley RJ, Purssell CP, Billson DR, Hutchins DA. A simple, low-cost conductive composite material for 3D printing of electronic sensors. *PloS one* 7; 2012: e49365.

[182] Farahani RD, Dalir H, Le Borgne V, Gautier LA, El Khakani MA, Lévesque M, Therriault D. Direct-write fabrication of freestanding nanocomposite strain sensors *Nanotechnology*, 23; 2012: 085502.

$$\rho C_p \frac{\partial T}{\partial t} = k \left(\frac{\partial^2 T}{\partial x^2} + \frac{\partial^2 T}{\partial y^2} + \frac{\partial^2 T}{\partial z^2} \right)$$

$$T = T_c + (T_m - T_c) \frac{\Delta h}{\sqrt{\pi \phi t}} \exp\left(-\frac{Z^2}{4\phi t}\right)$$

$$\varepsilon_{th} = \alpha_e \Delta T$$

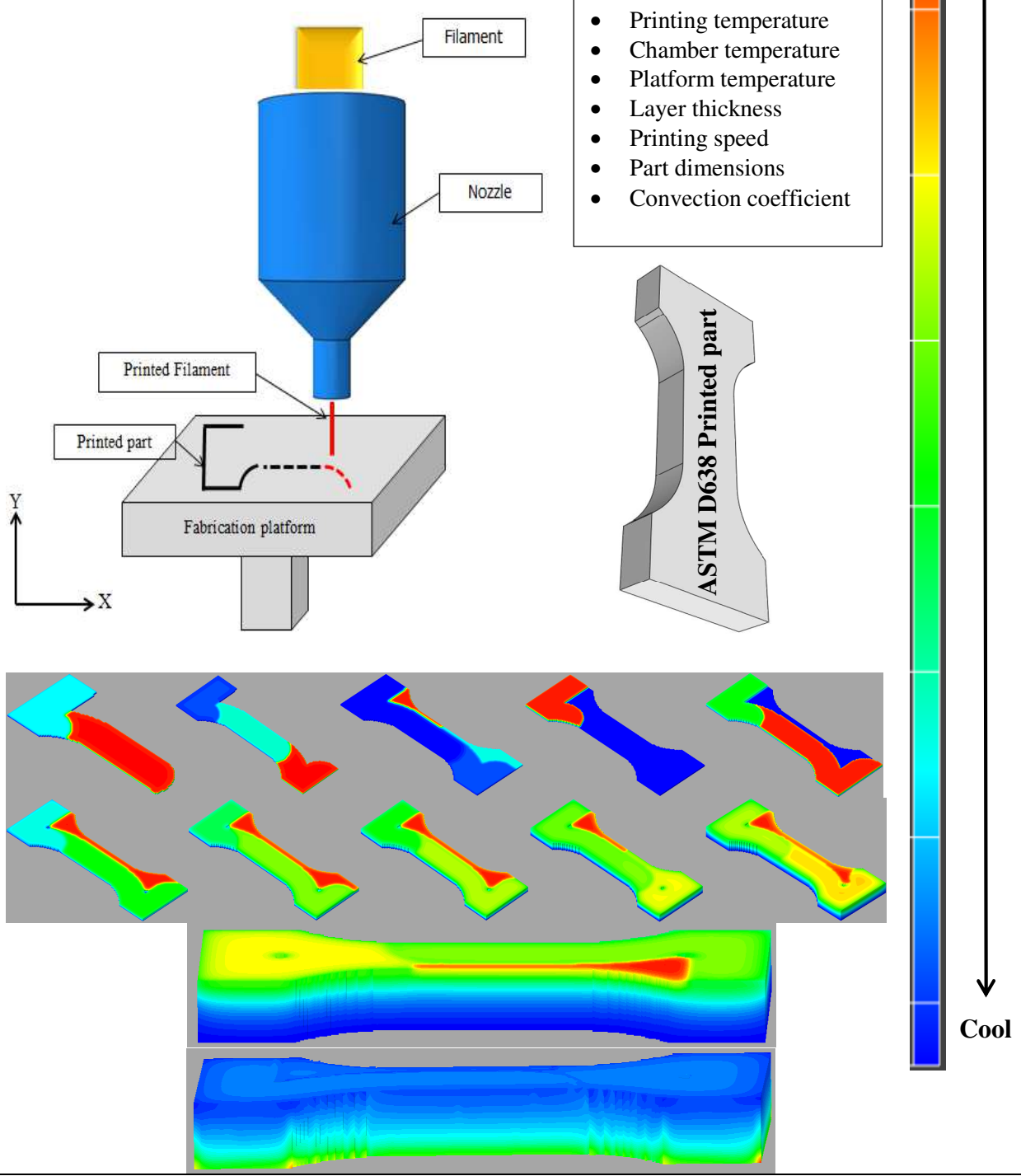


Figure: Additive manufacturing of polymer composites.